NASA Contractor Report 3940

Application of a Linearized Unsteady Aerodynamic Analysis to Standard Cascade Configurations

Joseph M. Verdon and William J. Usab, Jr.

CONTRACT NAS3-22257
JANUARY 1986

NASA

NASA Contractor Report 3940

Application of a Linearized Unsteady Aerodynamic Analysis to Standard Cascade Configurations

Joseph M. Verdon and William J. Usab, Jr.
United Technologies Research Center
East Hartford, Connecticut

Prepared for
Lewis Research Center
under Contract NAS3-22257

National Aeronautics
and Space Administration

**Scientific and Technical
Information Branch**

1986

Application of a Linearized Unsteady Aerodynamic Analysis to Standard Cascade Configurations

TABLE OF CONTENTS

	Page
SUMMARY	1
INTRODUCTION	3
THE LINEARIZED UNSTEADY AERODYNAMIC ANALYSIS	4
Governing Equations	4
Numerical Procedures	7
UNSTEADY EXCITATION AND RESPONSE PARAMETERS	9
THE STANDARD CASCADE CONFIGURATIONS	12
The First Standard Configuration	13
The Fifth Standard Configuration	14
The Eighth and Ninth Standard Configurations	15
THE NASA LEWIS FLUTTER CASCADE	17
CONCLUDING REMARKS	20
REFERENCES	22
LIST OF SYMBOLS	24
FIGURES	28

Application of a Linearized Unsteady Aerodynamic Analysis to Standard Cascade Configurations

SUMMARY

A linearized potential-flow analysis, which accounts for the effects of nonuniform steady flow phenomena on the linearized unsteady aerodynamic response to prescribed blade motions, has been applied to five cascade configurations. These include the first, fifth, eighth and ninth standard configurations proposed as a result of the Second International Symposium on Aeroelasticity in Turbomachines and a NASA Lewis flutter cascade. Selected results from this study, including comparisons between analytical predictions and the experimental measurements submitted for three of the foregoing configurations, are described in this report. The correlation between theory and experiment for the first standard configuration (a compressor cascade operating at low Mach number and frequency) is quite good. Moreover, the predictions and measurements for the NASA Lewis cascade of symmetric biconvex airfoils show good qualitative agreement. However, wide discrepancies exist between the theoretical predictions and the experimental measurements for the fifth standard configuration (a subsonic transonic fan tip cascade). These can be partially attributed to conditions being imposed in the experiment which differ from those commonly used in unsteady aerodynamic analyses.

INTRODUCTION

In the present study the linearized potential-flow analysis, described briefly in the next section and in detail in Refs. 1 through 4, has been used to determine unsteady response predictions for five cascade configurations. In particular, detailed unsteady response predictions have been determined for the first, fifth, eighth, and ninth standard configurations suggested by T. Fransson and P. Suter (Ref. 5) for theoretical and experimental investigations on turbomachine cascades. Similar theoretical results have also been determined for a NASA Lewis flutter cascade in support of the unsteady cascade experiments conducted at NASA Lewis Research Center (Ref. 6). In this report we summarize briefly our contribution to the establishment of the theoretical and experimental data base for the standard cascade configurations of Ref. 5. In addition, a detailed presentation of our theoretical results for the NASA Lewis cascade will be presented along with comparisons between these theoretical predictions and the measurements reported in Ref. 6.

The unsteady aerodynamic analysis used in this investigation (c.f. Refs. 1 through 4) applies to fan or compressor cascades operating at subsonic inlet Mach numbers. This analysis accounts for the effects of blade geometry, mean blade loading and transonic phenomena, including shocks and their motions, on the unsteady aerodynamic response to prescribed blade motions. The unsteady equations are derived from the assumption that unsteady disturbances are of small-amplitude and harmonic in time relative to a fully nonuniform irrotational mean or steady background flow. The resulting set of unsteady equations are linear, time-independent and contain variable coefficients which depend on the underlying mean flow. These equations are solved using an implicit least-squares finite-difference approximation which is applicable on arbitrary grids--an important feature for turbomachinery applications. In previous work numerical solutions, based on this linearized analysis, have been reported for subsonic flows through vibrating cascades of double-circular-arc (DCA) airfoils and NACA 0012 airfoils (Refs. 1 and 2), and for subsonic and transonic flows through vibrating cascades of flat-bottomed DCA airfoils (Refs. 3 and 4). More recently the unsteady analysis has been applied to representative two-dimensional outer-span sections of an actual fan rotor (Ref. 7). The results reported in Ref. 7 reveal dramatic effects of mean blade loading on the unsteady response to thin blades operating at high subsonic inlet Mach number and vibrating at high frequency.

The present study has been motivated by the need to assess the foregoing linearized unsteady aerodynamic analysis through comparisons between theoretical predictions and available experimental data. This exercise should serve to guide the improvements in numerical modeling that will be required to meet the goal of providing an efficient and reliable unsteady aerodynamic analysis, which can be used in turbomachinery aeroelastic design investigations.

THE LINEARIZED UNSTEADY AERODYNAMIC ANALYSIS

Governing Equations

We consider isentropic and irrotational flow of a perfect gas through a two-dimensional cascade (see Fig. 1) of vibrating airfoils. The blades are undergoing identical harmonic motions at frequency ω, but with a constant phase angle σ between the motions of adjacent blades. It is assumed that the flow remains attached to the blade surfaces and that the blade motion is the only source of unsteady excitation.

As a result of the foregoing assumptions the flow through the cascade is governed by the field equations

$$\frac{\partial \tilde{\rho}}{\partial t} + \nabla \cdot (\tilde{\rho} \nabla \tilde{\Phi}) = 0 \tag{1}$$

and

$$(\tilde{\rho}/\bar{\rho}_1) = 1 - (\gamma-1)\, \bar{\rho}_1 \{\tilde{\Phi}_t + [(\nabla\tilde{\Phi})^2 - V_1^2]/2\}/(\gamma P_1). \tag{2}$$

Here $\tilde{\Phi}(\vec{X},t)$ and $\tilde{\rho}(\vec{X},t)$ are the time-dependent velocity potential and fluid density; $\bar{\rho}_1$, P_1 and $\vec{V}_1$ are the upstream free-stream density, pressure and velocity respectively, γ is the specific heat ratio of the fluid, $\vec{X}$ is a position vector and t is time. In addition to Eqs. (1) and (2), the flow must be tangential to the moving blade surfaces and acoustic energy must either attenuate or propagate away from or parallel to the blade row in the far field. Finally, we also require that mass and tangential momentum be conserved across shocks and that pressure and the normal component of the fluid velocity be continuous across the vortex-sheet unsteady wakes which eminate from the blade trailing edges and extend downstream.

Equations (1) and (2) along with the equations based on the foregoing conditions at blade, shock and wake surfaces and in the far field are sufficient to determine the unsteady flow. However, the computing resources required by this nonlinear time-dependent unsteady aerodynamic formulation limits it usefulness for turbomachinery aeroelastic investigations. Instead, a small-unsteady-disturbance assumption is usually invoked. This assumption permits an efficient approximate description of the unsteady flow which is suitable for aeroelastic calculations.

Thus, following the approach used in Refs. 1-4, we assume that the blades are undergoing small-amplitude (i.e., of $\mathcal{O}(\varepsilon) \ll 1$) unsteady motions and expand the flow variables in asymptotic series in ε; e.g.,

$$\tilde{\Phi}(X,t) = \Phi(\vec{X}) + \tilde{\phi}(\vec{x},t) + \ldots . \tag{3}$$

Here, $\Phi(\vec{X})$ is the zeroth-order or steady-flow potential, $\tilde{\phi}(\vec{X},t) = \text{Re}\{\phi(\vec{X})e^{i\omega t}\}$ is the first-order (in ε) unsteady perturbation potential produced by harmonic blade motions, the dots refer to the higher-order terms and Re { } denotes the real part of { }. In addition to (3), Taylor series expansions are used to refer information on moving blade, shock and wake surfaces to the respective mean positions of these surfaces. After substituting these expansions into the full governing equations, equating terms of like power in ε, and neglecting terms of higher than first order in ε, time-independent nonlinear and linear variable-coefficient boundary-value problems are obtained, respectively, for the zeroth- and first-order flows.

The field equations governing the steady flow follow from Eqs. (1) and (2) after replacing the time-dependent variables $\tilde{\Phi}(\vec{X},t)$ and $\tilde{\rho}(\vec{X},t)$ by their zeroth-order or steady-flow counterparts $\Phi(\vec{X})$ and $\bar{\rho}(\vec{X})$, and setting temporal derivative terms equal to zero. The resulting equations, when combined with the associated zeroth-order boundary condition of flow tangency at the mean blade surfaces, prescribed uniform flow conditions at the inflow boundary, and a Kutta condition at blade trailing edges, describe the steady background flow through the stationary cascade.

The differential equation governing the first-order or linearized unsteady flow, i.e.,

$$A^2\nabla^2\phi = \frac{D_S^2}{Dt^2}\phi + (\gamma-1)\,\nabla^2\Phi\,\frac{D_S}{Dt}\phi + \nabla(\nabla\Phi)^2\cdot\nabla\phi/2, \tag{4}$$

follows from the mass conservation law (1), Bernoulli's equation (2), the isentropic relations, and the asymptotic expansions for the flow variables. Here $A = \gamma P/\bar{\rho}$ is the speed of sound propagation in the steady background flow, $D_S/Dt = i\omega + \nabla\Phi\cdot\nabla$ is a mean flow convection derivative operator and ϕ is the complex amplitude of the linearized unsteady potential. Solutions to Eq. (4) are

subject to both boundary conditions at the mean positions of the blade, shock and wake surfaces and requirements on the behavior of the unsteady disturbances far upstream and downstream from the blade row. Shock and wake (i.e., the steady downstream stagnation streamlines) mean positions are determined from the steady solution. The unsteady surface and far-field conditions are given explicitly in Refs. 1-4 and will not be repeated here.

The preceding aerodynamic formulation for determining the unsteady flow through a cascade of airfoils undergoing small-amplitude harmonic oscillations requires the solution of a nonlinear boundary-value problem for the zeroth-order or steady flow, followed by the solution of a linear variable-coefficient boundary-value problem for the first-order or linearized unsteady flow. Both of these problems are time-independent. Moreover, because of the cascade geometry and the assumed form of the blade motion, the steady and linearized unsteady flows must exhibit blade-to-blade periodicity. Thus; for example,

$$P(\vec{X} + m\tau\vec{e}_\eta) = P(\vec{X}) \tag{5}$$

and

$$p(\vec{X} + m\tau\vec{e}_\eta) = P(\vec{X})\, e^{im\sigma}, \tag{6}$$

where $P(\vec{X})$ is the steady pressure, $p(\vec{X})$ is the complex amplitude of the linearized unsteady pressure, $m = 0, \pm 1, \pm 2, \ldots$ is a blade number index, τ is the blade spacing and $\vec{e}_\eta$ is a unit vector in the "circumferential" or η-direction (see Fig. 1).

Conditions (5) and (6) allow a numerical resolution of the steady and the linearized unsteady flow equations to be restricted to a single extended blade-passage region of the cascade. Although the unsteady solution is dependent on the steady solution, the numerical procedures used to solve the two equation sets can be independent of each other. The numerical approximations used in the present study are described briefly below with primary emphasis placed on the unsteady solution procedure.

Numerical Procedures

In view of the stringent and often conflicting requirements placed on the construction of a computational mesh suitable for the resolution of cascade flow fields, numerical approximations to the steady (Refs. 8 and 9) and the linearized unsteady (Refs. 1-4) problems have been based on a two-step solution procedure. First, large-scale phenomena are determined on a sheared H-type cascade mesh of moderate density. Then, for blades with rounded leading edges or flows containing shocks, the second step is to determine detailed local solutions on body-fitted polar-type meshes of high density. The local mesh domains are chosen to cover and extend well beyond limited regions of high mean-velocity gradient. The final solutions to the steady and unsteady boundary-value problems are taken to be composites of the corresponding cascade- and local-mesh solutions.

The steady or mean flow solutions reported herein were determined using the two-dimensional finite-area approximation described in Refs. 8 and 9. In this method the integral form of the continuity equation is approximated over polygons in the physical plane. These polygons are constructed by a triangularization of the computational mesh. For transonic flows artificial compressibility is introduced in supersonic regions to stabilize the solution scheme and to capture shocks.

The unsteady solutions were determined using the finite-difference approximation described in Refs. 1-4. In this approach, discrete approximations to the linear unsteady equations are obtained using an implicit least-squares interpolation procedure. Thus, an algebraic approximation, $L\phi$, to the linear differential operator, $\mathcal{L}\phi$, at the mesh point, Q_0, is written in terms of the values of ϕ at Q_0 and at certain neighboring points $Q_1, \ldots, Q_N$ as follows

$$(\mathcal{L}\phi)_0 = (L\phi) = q^0\phi_0 + \sum_{n=1}^{N} \delta_n (\phi_n - \phi_0). \tag{7}$$

The difference coefficients δ_n in Eq. (7) are evaluated in terms of a prescribed set of interpolating functions and a set of interpolating coefficients. The latter are determined by a weighted least-squares procedure.

The points Q_0 through Q_N, termed a neighbor set, are defined in a "centered" fashion for interior or field points and in a one-sided fashion for boundary points. For transonic applications one must distinguish between regions of

subsonic flow, where the unsteady differential equation is elliptic, and supersonic flow, where it is hyperbolic. This change in equation type depends on the local mean-flow Mach number and is accommodated through the use of local type-dependent differencing approximations (see Refs. 3 and 4). With proper ordering the discrete unsteady equations can be assembled into a single block-pentadiagonal system, which can be solved conveniently using Gaussian elimination.

UNSTEADY EXCITATION AND RESPONSE PARAMETERS

In each of the aeroelastic cases considered here the unsteady excitation is due to blades undergoing prescribed single-degree-of-freedom torsional (pitching) motions about an axis at or near midchord. Furthermore, the blades are assumed to vibrate at a frequency ω (or a reduced frequency k based on blade semi-chord) with a constant phase angle σ between the motions of adjacent blades. Thus the angular displacement, $\tilde{\alpha}_m(t)$, of the mth blade is given by

$$\tilde{\alpha}_m(t) = \mathrm{Re}\{\alpha_m e^{i\omega t}\} = \mathrm{Re}\{\alpha_0 e^{i(\omega t+m\sigma)}\}, \quad m=0,\pm1,\pm2,\ldots, \tag{8}$$

where α_m is the complex amplitude of the mth blade angular displacement.

The linearized unsteady response parameters obey relations similar to (8) and thus it is only necessary to consider the response parameters associated with the reference blade. For convenience the subscript m = 0, which refers to the reference blade, will be omitted in the following discussion. The unsteady aerodynamic response quantities of interest include the perturbation unsteady pressure and pressure-difference coefficients, $\tilde{C}_p$ and $\Delta\tilde{C}_p$, respectively; the unsteady aerodynamic moment coefficient, $\tilde{C}_m$, acting an the moving reference blade surface; the aerodynamic work done by the airstream on this blade over one cycle of its motion, C_w; and the aerodynamic damping, coefficient, Ξ. These quantities are defined below.

The perturbation unsteady pressure coefficient at the moving reference blade surface is given by

$$\begin{aligned}\tilde{C}_p(x,t) &= \mathrm{Re}\{C_p(x)e^{i\omega t}\} = \mathrm{Re}\{|C_p|e^{i(\omega t+\phi_p)}\} \\ &= p_{\mathcal{B}}(x,t) \Big/ \left(\frac{1}{2}\bar{\rho}_1 V_1^2 \, |\alpha|\right), \quad 0 \le x \le c,\end{aligned} \tag{9}$$

where $C_p(x)$ is the complex amplitude of this pressure coefficient, x is a coordinate measuring distance along the mean blade-chord line, $|\ |$ denotes the magnitude of a complex quantity and ϕ_p is the phase angle by which the complex vector $C_p(x)$ leads the complex-displacement vector α. Furthermore, $p_{\mathcal{B}}(x,t)$ is the unsteady pressure perturbation at the instantaneous position of the reference blade surface $\mathcal{B}$, which is determined theoretically from the solutions for the steady and linearized unsteady veloicty potentials; ρ_1 and V_1 are the uniform

density and flow speed, respectively, far-upstream of the cascade (see Fig. 1); and c is the blade chord length. The unsteady pressure-difference coefficient is defined by

$$\tilde{\Delta C}_p(x,t) = \mathrm{Re}\{\Delta C_p(x)e^{i\omega t}\} = \mathrm{Re}\{|\Delta C_p|e^{i(\omega t+\phi_{\Delta p})}\}$$

$$= \tilde{C}_p(x_-,t) - \tilde{C}_p(x_+,t) \quad , 0 \leq x \leq c, \tag{10}$$

where the subscripts - and + refer to the lower (pressure) and upper (suction) surfaces of the blade respectively, and $\phi_{\Delta p}$ is the phase angle by which the complex pressure difference, ΔC_p, leads the complex angular displacement, α.

The perturbation unsteady moment coefficient is defined by

$$\tilde{C}_m(t) = \mathrm{Re}\{C_m e^{i\omega t}\} = \mathrm{Re}\{|C_m|e^{i(\omega t+\phi_m)}\}$$

$$= -c^{-2}\oint_{\mathcal{B}} \tilde{C}_p(x,t)(\vec{R}_p \cdot d\vec{s}), \tag{11}$$

where ϕ_m is the phase angle by which the moment leads the angular displacement, $\vec{R}_p$ is a position vector extending from the reference blade axis of rotation to a point on the moving reference blade surface and $d\vec{s}$ is a differential vector tangent to this blade surface and directed counterclockwise. Both the angular displacement and the moment are regarded here as being positive in the clockwise direction. It should be noted that, if shock discontinuities are present, additional terms must be added to the right-hand-sides of Eqs. (9) and (11) to account for the concentrated loads produced by the motions of the shocks along the blade surface (see Refs. 3 and 4).

Finally, the aerodynamic work per cycle and the aerodynamic damping coefficient for the pure torsional vibrations are given by

$$C_w = -\pi|\alpha|\Xi = \pi|\alpha||C_m|\sin\phi_m. \tag{12}$$

When α is prescribed as a real quantity, the right-hand-side of Eq. (12) can be

replaced by $\pi\alpha \mathrm{Im}\{C_m\}$, where $\mathrm{Im}\{\ \}$ denotes the imaginary part of $\{\ \}$. The stability of the torsional blade motion (according to linearized theory) depends upon whether $C_w \lessgtr 0$ (or $\Xi \gtrless 0$). Thus, if $C_w < 0$, the airstream removes energy from the blade motion and this motion is stable; if $C_w = 0$, there is no net transfer of energy and the blade motion is neutrally stable; and finally, if $C_w > 0$, the airstream supplies energy to the blade motion and this motion is unstable.

THE STANDARD CASCADE CONFIGURATIONS

At the Second International Symposium on Aeroelasticity in Turbomachines held in Lausanne, Switzerland in September 1980 (Ref. 10), it was proposed that an experimental and analytical data base be established for selected turbomachine-cascade configurations. The purposes of this effort are: first, to provide a convenient means for evaluating and comparing the results of different theoretical analyses; and second, to provide a convenient means for assessing theoretical predictions through comparisons with experimental measurements. In the four year period between the Second Symposium and the Third Symposium, held in Cambridge, U.K., nine two-dimensional and quasi three-dimensional standard cascade configurations were proposed, and the developers of various theoretical models were asked to apply their calculation methods to predict the aeroelastic behavior of these configurations.

The present authors have contributed to this project by applying the unsteady aerodynamic analysis of Refs. 1 through 4 to predict unsteady aerodynamic response properties for the following two-dimensional cascade configurations:

(1) a compressor cascade consisting of cambered NACA 65 series airfoils and referred to in Ref. 5 as the first standard configuration;

(2) a subsonic/transonic fan-tip cascade, referred to as the fifth standard configuration;

(3) a cascade of flat plate airfoils, referred to as the eighth standard configuration; and

(4) a cascade of double-circular-arc airfoils referred to as the ninth standard configuration.

These standard configurations, along with the recommended aeroelastic test cases, are described in detail in Ref. 5. We determined unsteady aerodynamic response information for fifteen (15) recommended test cases on the first, eighth and ninth configurations, and for eight (8) cases on the fifth configuration for a total of fifty-three (53) test cases.

Our results were submitted to T. H. Fransson for inclusion in a paper (Ref. 11) that he presented at the Third Symposium. In addition, one of the present authors (J. M. Verdon) attended this Symposium to give a brief presentation describing the linearized unsteady potential-flow analysis used in our study and the application of this analysis to the four standard configurations listed above. A sample of our results are included in Figs. 1 through 4 of Ref. 11. These figures contain our predictions (referred to as Code 3) as well as the

analytical predictions and the experimental data contributed by other investigators. A more complete report on the analytical and experimental results submitted on the standard configurations is being prepared by Fransson for publication later this year. In view of this, a detailed presentation of our results will not be given in this report. But we will include a representative selection of these results, including several based on more recent calculations, and offer some general observations on the analytical and experimental results presented at the Third Symposium for the standard configurations listed above.

The First Standard Configuration

The first standard configuration is a compressor-type cascade operating at low subsonic inlet Mach number (M_1). This cascade has a 35° stagger angle (θ in Fig. 1) and a gap to chord ratio τ/c of 0.75. The blades are constructed by superimposing a NACA 65 series thickness distribution on a 10 degree circular-arc camber line. They are driven in the torsional mode at amplitudes, $|\alpha|$, of 0.5° and 2.0° around an axis at (x/c,y/c) = (0.5, 0.115) and at frequencies varying from 9 to 77 Hz (i.e., semi-chord reduced frequencies, k, between 0.072 and 0.603). Most of the tests were conducted at 15.5 Hz (k = 0.122). The experiments were conducted by F. O. Carta (Ref. 12) in the UTRC Oscillating Cascade Wind Tunnel and three investigators contributed theoretical predictions.

In general, the theoretical analyses predicted the measured unsteady aerodynamic response behavior quite well, both in terms of the detailed unsteady pressure information along a blade surface and the global unsteady response quantities (unsteady moment, etc.). However, there is some ambiguity concerning the inlet flow angle (β_1). Theoretical predictions for mean surface pressures have been found to match closely the corresponding measured pressures, but only if the inlet flow angle prescribed for the theoretical calculation differs from that reported in the experiment. The present authors have found that a similar situation also exists for the fifth standard configuration.

A sample of our predictions along with Carta's measurements for the mean pressure coefficient, C_p, on the reference blade surface, the unsteady pressure coefficient, the unsteady pressure-difference coefficient, and the unsteady moment are shown in Figs. 2 through 5, respectively. The mean pressure coefficient is defined by

$$\bar{C}_p(x) = \left(P(x) - P_1\right) \Big/ \left(\frac{1}{2}\,\bar{\rho}_1 V_1^2\right) \tag{13}$$

The analytical and experimental results shown in Figs. 2 through 5 are in very good agreement. They were determined for an inlet Mach number of 0.17 and blades

vibrating with $\alpha = 2°$ and at a reduced frequency of 0.122. The inlet flow angle used in the analysis is 27.8°, while that reported for the experiment is 24°. It should be noted that the theoretical moment curve shown in Fig. 5 was determined recently on the basis of moment predictions for forty values of σ, so that a detailed description of the unsteady moment behavior, especially in the super-resonant region near $\sigma = 0°$, could be provided. Results for only nine values of σ, corresponding to those at which measurements are available, were submitted at the Third Symposium.

The Fifth Standard Configuration

The fifth standard configuration is a two-dimensional subsonic/transonic fan tip cascade which has been tested in a rectilinear cascade wind tunnel at ONERA by Szychenyi and Finas (Ref. 13). The experimental configuration consists of six thin uncambered blades having a maximum thickness to chord ratio of 0.027 at approximately 67% of blade chord. The cascade stagger angle, θ, is 30.7° and the gap to chord ratio, τ/c, is 0.95. The experiments were performed for torsional motions about midchord with $|\alpha| = 0.3°$ and over a frequency range extending from 75 (k= 0.14) to 550 (k = 1.02) Hz. The inlet Mach number was varied from 0.5 to 1.0, and the inlet flow angle was varied from 28.7° to 18.7°, corresponding to attached through fully separated flow. Unfortunately, only one blade was vibrated in the experiments. Although methods are available for converting the resulting unsteady response information to represent that for a cascade with all blades vibrating, these were not applied and therefore some questions remain concerning the validity of the comparisons between the data and the analytical predictions for the fifth standard configuration.

Two theoretical models (c.f. Refs. 1-4 and Ref. 14) were applied to provide predictions for $M_1 = 0.5$ in the attached (experimental $\beta_1 = 26.7°$) and partly-separated (experimental $\beta_1 = 24.7°$) flow domains. No predictions were submitted for the fully-stalled experimental conditions. There are large differences between the predicted and measured values for the magnitudes of the unsteady pressures, pressure differences and aerodynamic moments. Moreover, substantial differences also exist between the results of the two theoretical prediction methods for these quantities. However, the two analytical and the experimental results for the phase angles between the unsteady surface pressure, pressure difference and aerodynamic moment and the angular displacement are in reasonably good agreement. Consequently, both theory and experiment give the same indication in regard to the stability of the torsional blade motions. The differences between the theoretical predictions and the measurements can perhaps be attributed to viscous separation phenomena which are present in the experiment but are not accounted for in the theoretical models. In addition, only one blade was excited in the finite-cascade experiment while all blades are assumed to be oscillating in the infinite-cascade theoretical formulations. The reasons for

the differences between the predictions of the two theoretical models are not apparent at the present time.

A selection of our results for mean surface-pressure coefficient, unsteady pressure-difference coefficient and aerodynamic damping are shown in Figs. 6 through 8 along with the data contributed by Szychenyi. Substantial differences exist between the predictions and measurements for the mean-pressure coefficient near the leading edge of the blade (Fig. 1) and for the magnitude of the unsteady pressure-difference coefficient over the entire blade. Good agreement exists between the theoretical and experimental values for the phase angle, $\phi_{\Delta p}$, and the aerodynamic damping, Ξ, for the partly-separated flow, but this must be regarded as fortuitous in view of the discrepancies between the analytical and experimental results for $|\Delta C_p(x)|$.

The Eighth and Ninth Standard Configurations

The eighth and ninth configurations were selected for the validation of various theoretical prediction methods, especially at high subsonic inlet Mach number. Therefore, no experimental results were submitted for these standard configurations. The eighth configuration is a two-dimensional cascade of flat-plate blades. The blades undergo torsional oscillations about midchord at relatively high reduced frequency (i.e., $k = 1.0$), and the phase angle between the motion of adjacent blades is 90°. The cascade stagger angle and gap/chord ratio are variable, but for most of the test cases $\theta = 30°$ and $\tau/c = 0.75$. The inlet Mach number varies from 0 to 1.5, and in each case the inlet flow angle is set equal to the cascade stagger angle and therefore the mean flow is uniform.

The present authors submitted results only for subsonic inlet Mach numbers with M_1 extending from 0.1 to 0.95. Three other investigators also submitted theoretical predictions for this Mach number range. The results of the various prediction methods for the subsonic flat-plate cascades are generally in good agreement. However, there are some discrepancies between the predictions for $|C_p|$ at high subsonic inlet Mach number. These are due, perhaps, to the difficulties associated with the numerical prediction of high-frequency unsteady flow at high subsonic Mach number. Our results for the unsteady pressure-difference coefficient at $M_1 = 0.8$ and unsteady moment versus inlet Mach number are given in Figs. 9 and 10, respectively. The results of the other prediction methods are in good agreement with those presented in these figures.

The ninth configuration is a two-dimensional cascade of double-circular-arc airfoils. Both symmetric and flat-bottomed DCA airfoils have been recommended. In the symmetric case the blade thickness varies from one to ten percent of chord, while the flat-bottomed blades are 5% thick. The cascade gap to chord

ratio is 0.75 and there are two stagger angles, $\theta = 30°$ and $\theta = 45°$. The blades undergo torsional oscillations about midchord at a reduced frequency, k, of 1.0. The inlet Mach number varies from 0 to 1.5, and the inlet flow angle is determined by prescribing a unique mean-incidence condition at blade leading edges.

The results of two theoretical analyses (Refs. 1-4 and Ref. 14) were submitted for subsonic flow through the symmetric DCA configurations. The present authors also contributed results for subsonic and discontinuous transonic flows through the cascade of flat-bottomed DCA airfoils; however, we did not submit results for supersonic inlet conditions. The results of the two analyses for subsonic flows through the cascades of symmetric DCA blades are generally in good agreement, but increasing differences are observed with increasing inlet Mach number and/or blade thickness. Our results for the unsteady pressure-difference coefficient and for the unsteady moment versus inlet Mach number for a cascade of 2% thick blades are shown in Figs. 11 and 12. The results of the other prediction method are in close agreement with those shown in these figures. Again, we note that the moment curves shown in Figs. 10 and 12 are based on recent more detailed calculations than those submitted for the Third Symposium.

THE NASA LEWIS FLUTTER CASCADE

The NASA Lewis flutter cascade consists of nine uncambered or symmetric biconvex airfoils which are driven simultaneously to provide a 1.2° amplitude pitching motion about midchord. The cascade has a stagger angle of 37° and a gap/chord ratio of 0.767. The symmetric biconvex airfoils are 7.62 cm. long, and they have a maximum thickness at midchord of 0.58 cm. The radius of curvature of the upper (suction) and lower (pressure) surfaces is 27.4 cm. The experimental airfoils close in rounded leading and trailing edge sections of radius 0.000254 cm. Tests were performed at an inlet Mach number of 0.65 and an inlet flow angle of 0° in an attempt to simulate an unloaded and shock-free mean-flow condition. Tests were also performed at an inlet Mach number of 0.8 and an inlet flow angle of 30° in order to observe the surface-pressure response when an oscillating shock occurs near the leading edge of each airfoil. The unsteady response data are given in Ref. 6 for torsional vibrations about midchord at interblade phase angles of -90° and +90° and vibration frequencies of 200 Hz and 500 Hz (i.e., semi-chord reduced frequencies of k = 0.221 and 0.553 for M_1 = 0.65, and k = 0.183 and 0.458 for M_1 = 0.80).

Analytical results for the NASA Lewis Cascade are depicted, along with the measurements of Ref. 6, in Figs. 13 through 26 of the present report. The blades used in the analytical study are extended versions of those used in the experiment. That is, sharp-edged biconvex (or symmetric DCA) blades having the same surface radius and the same thickness at midchord as those used in the experiment were employed, but the upper and lower surfaces of the blades used in the analysis were extended to close in wedge-shaped leading and trailing edges. As a result the blades used in the analysis are 4% longer than those used in the experiment. This modification was introduced to simplify analytical considerations at blade edges. With the exception of the inlet flow angle for the M_1 = 0.65 case, all other experimental parameters have been retained in the analytical study. The steady full-potential analysis (Refs. 8 and 9) used in this study indicates that, for M_1 = 0.65, the unloaded mean-flow condition occurs at β_1 = 33.22° and not at β_1 = 37°, as reported in the experiment. After a number of unsuccessful attempts to match the measured blade-surface Mach number distributions by prescribing different combinations of inlet and exit flow angles, we decided to provide analytical predictions at M_1 = 0.65 for the unloaded mean-flow condition. These results should provide useful "benchmark" information for use in possible future experiments.

The predicted and measured unsteady response information for M_1 = 0.65 are shown in Figs. 13 through 19. As mentioned, the analytical predictions correspond to an inlet flow angle of 33.22° while the inlet flow angle reported in the

experiment is 37.0°. The predicted steady Mach number distributions in Fig. 13 correspond to the zero mean blade-loading condition, while the experimental Mach number distributions indicate that a negative steady lift force acts on each blade. Although the analytical steady background flow differs from that occurring in the experiment, the mean-flow gradients are relatively small in both instances and are not expected to have a major impact on the unsteady response. It is therefore still meaningful to compare the predicted and measured unsteady response information.

The predicted and measured unsteady surface pressures are shown in Figs. 14 through 17 for the following combinations of frequency and interblade phase angle: ω = 200 Hz and $\sigma = -90°$ (Fig. 14); ω = 200 Hz and $\sigma = 90°$ (Fig. 15); ω = 500 Hz and $\sigma = -90°$ (Fig. 16); and ω = 500 Hz and $\sigma = 90°$ (Fig. 17). With the exception of the latter combination, which is close to a resonance condition (see Fig. 19), a qualitative agreement between the measured and predicted unsteady surface pressures has been achieved. The predicted behavior of the unsteady moment coefficient versus interblade phase angle is illustrated, along with the experimental values at $\sigma = \pm 90°$, in Fig. 18 for ω = 200 Hz and in Fig. 19 for ω = 500 Hz. It should be noted that the experimental moment coefficients were estimated from unsteady pressure-response data available at only six points on the blade suction surface and six points on the blade pressure surface. Hence, the experimental estimates for the unsteady moment coefficients may not be too reliable. However, with the exception of the motion at ω = 200 Hz and $\sigma = 90°$ (Fig. 18), the in-phase components ($\mathrm{Re}\{C_m\}$) of the analytical and experimental moments are in good agreement. The out-of-phase components ($\mathrm{Im}\{C_m\}$) are also in good agreement for $\sigma = 90°$, but appreciable differences exist at $\sigma = -90°$ (see Figs. 18 and 19).

Similar results are provided in Figs. 20 through 26 for the high inlet Mach number ($M_1 = 0.8$), high mean incidence ($\beta_1 = 30°$) condition. In this case the analytical predictions in the vicinity of the blade leading edge are questionable because the steady and unsteady flow behavior in the vicinity of a sharp leading edge at incidence cannot be predicted adequately. Indeed, unless a relatively coarse computational grid is employed near the leading edge of a blade, iterative solution procedures for the steady full-potential equation will diverge. It is therefore not possible to predict the unsteady effects associated with certain phenomena observed in the experiment (Ref. 6), e.g., leading-edge lambda-type shocks and flow separations downstream of these shocks, using the current inviscid steady and unsteady codes.

In view of these limitations the correlation between the predicted and measured surface Mach number distributions, shown in Fig. 20, is encouraging. The predicted and measured unsteady surface-pressure coefficients for torsional vibrations about midchord, at the same combinations of frequency and interblade phase angle considered above, are shown in Figs. 21 through 24. Again, with the exception of the motion at ω = 500 Hz and $\sigma = 90°$, which is near a resonance

condition, there is a reasonable qualitative agreement between the predicted and measured surface-pressure coefficients. However, large differences do exist over the forward part of the blade suction surface. The predicted and measured (at $\sigma = \pm 90°$) unsteady moment coefficients for the flows at $M_1 = 0.8$ are shown in Fig. 25 for $\omega = 200$ Hz and in Fig. 26 for $\omega = 500$ Hz.

CONCLUDING REMARKS

This report describes a theoretical contribution to the establishment of a theoretical and experimental data base for the validation of current and future unsteady flow analyses. In particular, the linearized potential-flow analysis of Refs. 1 through 4 has been applied to provide unsteady aerodynamic response predictions for five two-dimensional compressor (or fan) - type cascade configurations. These include the first, fifth, eighth and ninth standard cascade configurations of Ref. 5 and the NASA Lewis flutter cascade of Ref. 6. Unsteady response measurements are available for the first and fifth standard configurations and for the NASA Lewis cascade; several other investigators have contributed theoretical predictions for the standard cascade configurations.

Our predictions have been found to be in very good agreement with those of other theoretical investigators for the first (a cascade of NACA 65 series airfoils), eighth (a flat-plate cascade) and ninth (a cascade of double-circular-arc airfoils) standard configurations (see Ref. 11), and with the experimental measurements of Ref. 12 for the first standard configuration. In addition, good qualitative agreement exists between our predictions and the experimental measurements of Ref. 6 for the NASA Lewis configuration (a cascade of symmetric biconvex airfoils). However, wide discrepancies exist between the predicted and measured values for the magnitudes of the complex response quantities for the fifth standard configuration. These are due, possibly, to the different conditions which prevail in the experimental (only one blade vibrating) and the analytical (all blades vibrating) flow environments.

In both the NASA Lewis and the fifth standard configurations the blades have very small leading-edge radii, and they operate at non-zero mean incidence. Thus, large flow gradients occur along each blade suction surface in the vicinity of its leading edge, and these promote shock formation and flow separation. At present it is not possible to resolve such detailed local phenomena with existing inviscid (or viscous) flow codes. Thus, we recommend that future research be directed toward improving inviscid steady and linearized unsteady flow codes so that transonic leading-edge phenomena can be predicted. In addition, the possibility of extending linearized unsteady aerodynamic formulations to account for viscid/inviscid interaction phenomena, including leading-edge and/or shock-induced separations, should be explored.

The concept of establishing a theoretical and experimental data base for standard cascade configurations, as proposed at the Second International Symposium on Aeroelasticity in Turbomachines, is an important one. Before the start of the Third Symposium, there were concentrated efforts on the part of both experimentalists and theoreticians, working independently, to submit measurements

and predictions for the various configurations. Such an approach is useful in getting started, especially if the measurements and predictions are found to be in close agreement. Usually this will not be the case, however, because of the complicated nature of the unsteady flows through turbomachinery blade rows. Thus, future activities of this kind would benefit from research programs in which theoreticians and experimentalists worked together from the outset. In such programs, benchmark analytical and experimental studies could be planned and conducted to identify carefully both the regions in which the results of theory and experiment will correlate and the additional physical phenomena that must be incorporated in theoretical models. Basic issues to be addressed are the determination of the ranges of validity of both the linearized unsteady aerodynamic analyses which have been developed for turbomachinery aeroelastic applications and the finite-cascade wind-tunnel experiments which are used to validate these analyses.

REFERENCES

1. Verdon, J. M. and J. R. Caspar: Development of an Unsteady Aerodynamic Analysis for Finite-Deflection Subsonic Cascades. NASA CR 3455, prepared under Contract NAS3-21981 for Lewis Research Center, September 1981.

2. Verdon, J. M. and J. R. Caspar: Development of a Linear Unsteady Aerodynamic Analysis for Finite-Deflection Subsonic Cascades. AIAA Journal, Vol. 20, No. 9, September 1982, pp. 1259-1267.

3. Verdon, J. M. and J. R. Caspar: A Linear Aerodynamic Analysis for Unsteady Transonic Cascades. NASA CR 3833, prepared under Contract NAS3-23696 for Lewis Research Center, September 1984.

4. Verdon, J. M. and J. R. Caspar: A Linearized Unsteady Aerodynamic Analysis for Transonic Cascades. Journal of Fluid Mechanics, Vol. 149, December 1984, pp. 403-429.

5. Fransson, T. H. and P. Suter: Two-Dimensional and Quasi-Three Dimensional Experimental Standard Configurations for Aeroelastic Investigations of Turbomachine Cascades. Report LTA-TM-83-2, Ecole Polytechnique Federale de Lausanne, Laboratorie de Thermique Appliquee, September, 1983.

6. Shaw, L. M., D. R. Boldman, A. E. Buggele, and D. H. Buffum: Unsteady Pressure Measurements on a Biconvex Airfoil in a Transonic Oscillating Cascade. Paper No. 85-GT-212, ASME 30th International Gas Turbine Conference and Exhibit, Houston, Texas, March 18-21, 1985.

7. Usab, W. J., Jr. and J. M. Verdon: On the Application of a Steady and a Linearized Unsteady Potential-Flow Analysis to Two-Dimensional Fan-Tip Cascades. UTRC Report R85-256556-1, February 1985.

8. Caspar, J. R., D. E. Hobbs and R. L. Davis: Calculation of Two-Dimensional Potential Cascade Flow Using Finite Area Methods. AIAA Journal, Vol. 18, January 1980, pp. 103-109.

9. Caspar, J. R.: Unconditionally Stable Calculation of Transonic Potential Flow Through Cascades Using an Adaptive Mesh for Shock Capture. Transactions of the ASME, Journal of Engineering for Power, Series A, Vol. 105, No. 3, July 1983, pp. 504-513.

10. Suter, P. (editor): Aeroelasticity in Turbomachines, Proceedings of the Second International Symposium held in Lausanne, Switzerland, September 8-12, 1980, Juris-Verlag, Zurich, 1981.

REFERENCES (Cont'd)

11. Fransson, T. H.: Workshop on Aeroelasticity in Turbomachine - Cascades. Cambridge Symposium Proceedings: Unsteady Aerodynamics of Turbomachines and Propellers, September 1984, pp. 361-395.

12. Carta, F. O.: Unsteady Aerodynamics and Gapwise Periodicity of Oscillating Cascaded Airfoils. Transactions of the ASME, Journal of Engineering for Power, Series A, Vol. 105, No. 3, July 1983, pp. 565-574.

13. Szechenyi, E. and R. Finas: Aeroelastic Testing in a Straight Cascade Wind Tunnel. Aeroelasticity in Turbomachines, P. Suter (editor), Proceedings of the Second International Symposium held in Lausanne, Switzerland, September 8-12, 1980, Juris-Verlag Zurich, 1981, pp. 143-150.

14. Whitehead, D. S.: The Calculation of Steady and Unsteady Transonic Flow in Cascades. Cambridge University Engineering Department Report CUED/A-Turbo/TR 118, 1982.

LIST OF SYMBOLS

Latin

A	Speed of sound propagation in the steady background flow, Eq. (4)
$\tilde{C}_m$	Perturbation unsteady moment coefficient, Eq. (11)
$\tilde{C}_p$	Perturbation unsteady surface pressure coefficient, Eq. (9)
$\overline{C}_p$	Steady pressure coefficient, Eq. (13)
C_m	Complex amplitude of the perturbation unsteady moment coefficient, Eq. (11)
C_p	Complex amplitude of the perturbation unsteady surface pressure coefficient, Eq. (9)
C_w	Aerodynamic work per cycle of blade motion, Eq. (12)
c	Blade chord length, Fig. 1
D_S/Dt	Mean-flow convective derivative operator, Eq. (4)
$\vec{ds}$	Differential vector tangent to blade surface and directed counterclockwise, Eq. (11)
$\vec{e}_\eta$	Unit vector in the cascade "circumferential" or η-direction, Eq. (5)
$\mathrm{Im}\{\ \}$	Imaginary part of { }
k	Reduced frequency based on blade semi-chord
$\mathcal{L}$	Linear differential operator, Eq. (7)
L	Linear difference operator, Eq. (7)
M	Zeroth-order or steady Mach number
m	Blade number index (m=0 denotes the reference blade)
N	Number of neighbor mesh points, Eq. (7)
n	Mesh point index, Eq. (7)
P	Zeroth-order or steady pressure, Eq. (5)

LIST OF SYMBOLS (Cont'd)

$P_{\mathcal{B}}$	Linearized unsteady pressure at the instantaneous position of the reference blade surface, Eq. (9)
p	Complex amplitude of first order or linearized unsteady pressure, Eq. (6)
Q_n	Mesh point, n=0 refers to calculation point, n=1,..., N refers to neighboring mesh points
q^0	Multiplicative constant, Eq. (7)
$\vec{R}_p$	Position vector extending from reference blade axis of rotation to points on the reference blade surface, Eq. (11)
Re{ }	Real part of { }, Eq. (3)
t	Time
$\vec{V}$	Zeroth-order or steady velocity, Eq. (2)
$\vec{X}$	Position vector
x	Distance from leading edge along blade chord, Fig. 1

Greek

$\tilde{\alpha}$	Blade angular displacement, Eq. (8)
α	Complex amplitude of the blade angular displacement, Eq. (8)
$\beta_{1,2}$	Inlet, exit flow angle, Fig. 1
γ	Specific heat ratio, Eq. (2)
$\Delta\tilde{C}_p$	Perturbation unsteady pressure-difference coefficient, Eq. (10)
ΔC_p	Complex amplitude of the perturbation unsteady pressure-difference coefficient, Eq. (10)

LIST OF SYMBOLS (Cont'd)

δ_n	Finite-difference coefficient, Eq. (7)
ε	Small parameter which is a measure of the amplitude of the blade motion
η	Cascade "circumferential" coordinate, Fig. 1
Θ	Cascade stagger angle, Fig. 1
Ξ	Aerodynamic damping coefficient, Eq. (12)
$\tilde{\rho}$	Nonlinear time-dependent fluid density, Eq. (1)
$\bar{\rho}$	Zeroth-order or steady density, Eq. (1)
σ	Interblade phase angle, positive when motion of the (m+1)th blade leads the motion of the mth blade, Eq. (8)
τ	Blade spacing, Fig. 1 and Eq. (5)
$\tilde{\Phi}$	Nonlinear time-dependent velocity potential, Eq. (1)
Φ	Zeroth-order or steady velocity potential, Eq. (3)
$\phi_{m,p,\Delta p}$	Phase angle by which a complex response vector (moment, pressure, pressure difference) leads the complex angular displacement vector, Eqs. (9), (10) and (11)
$\tilde{\phi}$	First-order or linearized unsteady velocity potential, Eq. (3)
ϕ	Complex amplitude of the linearized unsteady velocity potential, Eq. (4)
ω	Frequency of the blade motion, Eq. (8)

Subscripts

B	Instantaneous position of reference blade
m	Blade number index, Eq. (8)

LIST OF SYMBOLS (Cont'd)

n	Mesh point index, Eq. (7)
t	Partial derivative with respect to time, Eq.(1)
1	Uniform inlet flow condition, Eq. (2)
+,-	Upper, lower surface of blade, Eq. (10)

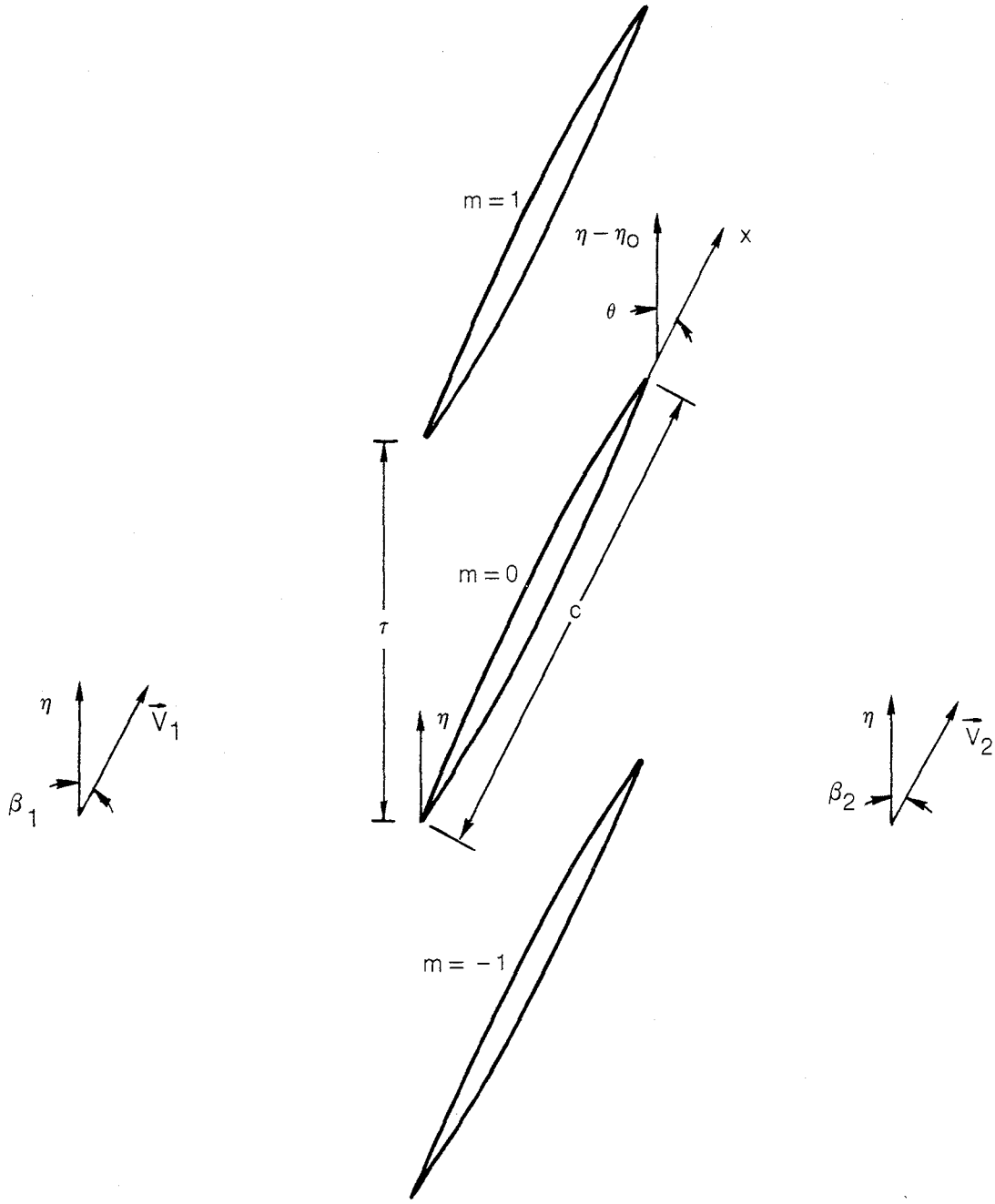

Fig 1 Two-Dimensional Cascade Nomenclature.

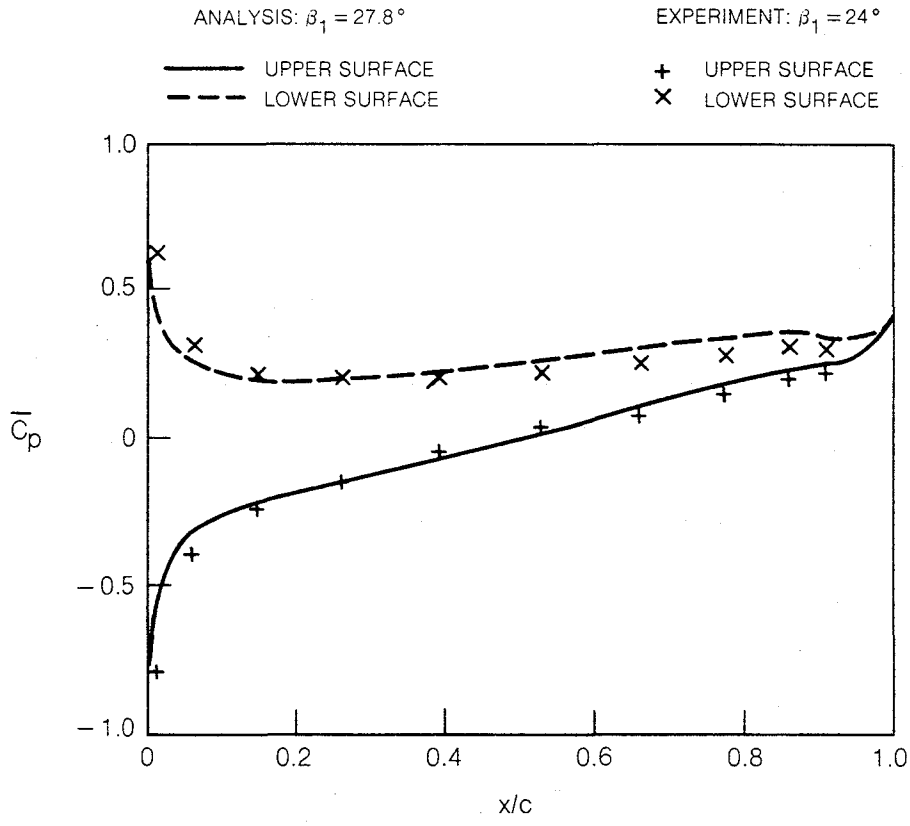

Fig. 2 Mean Surface-Pressure Coefficient for the First Standard Configuration; $M_1 = 0.17$.

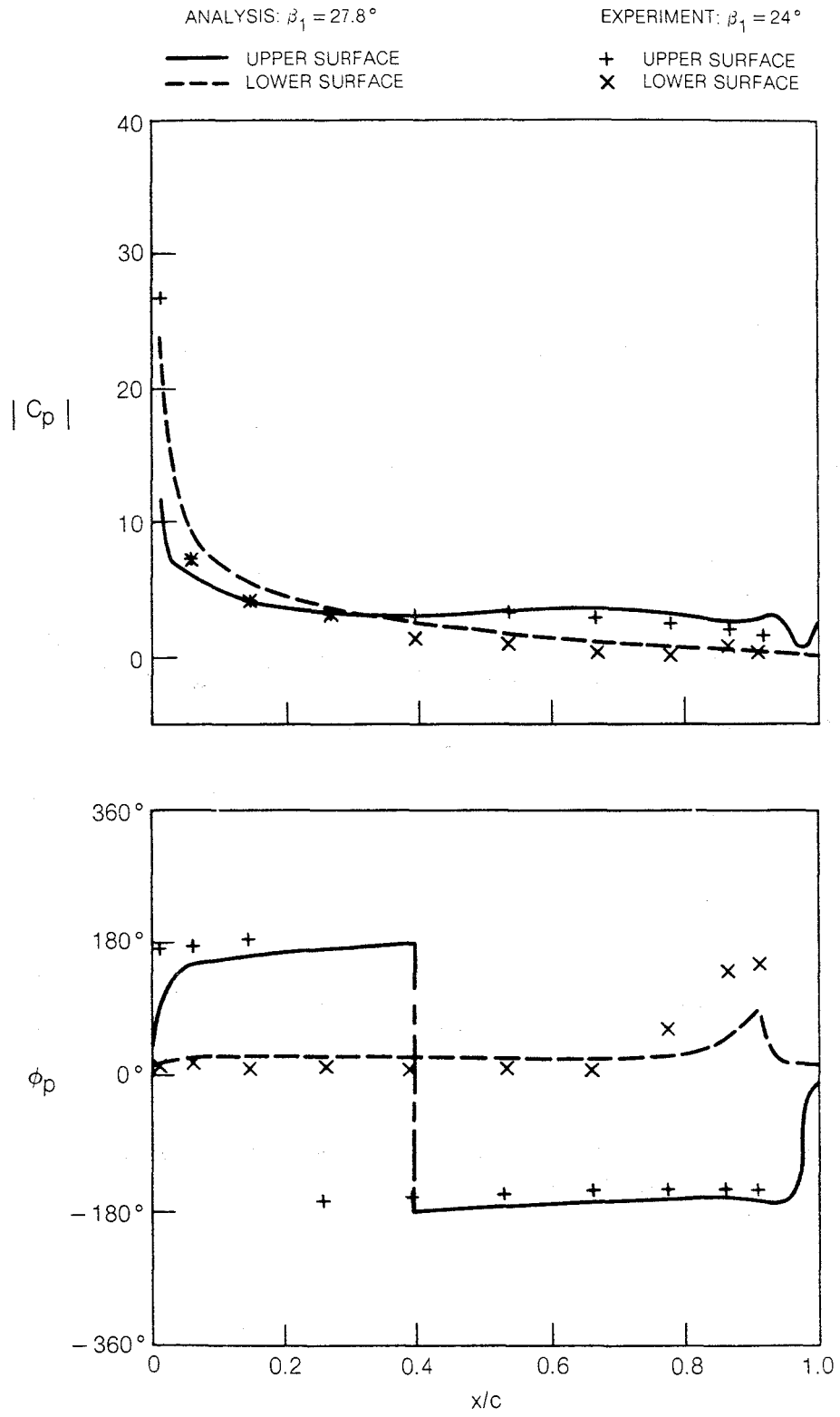

Fig. 3 Unsteady Surface-Pressure Coefficient for the First Standard Configuration; $M_1 = 0.17$, $\alpha = 2°$, $k = 0.122$, $\sigma = -135°$.

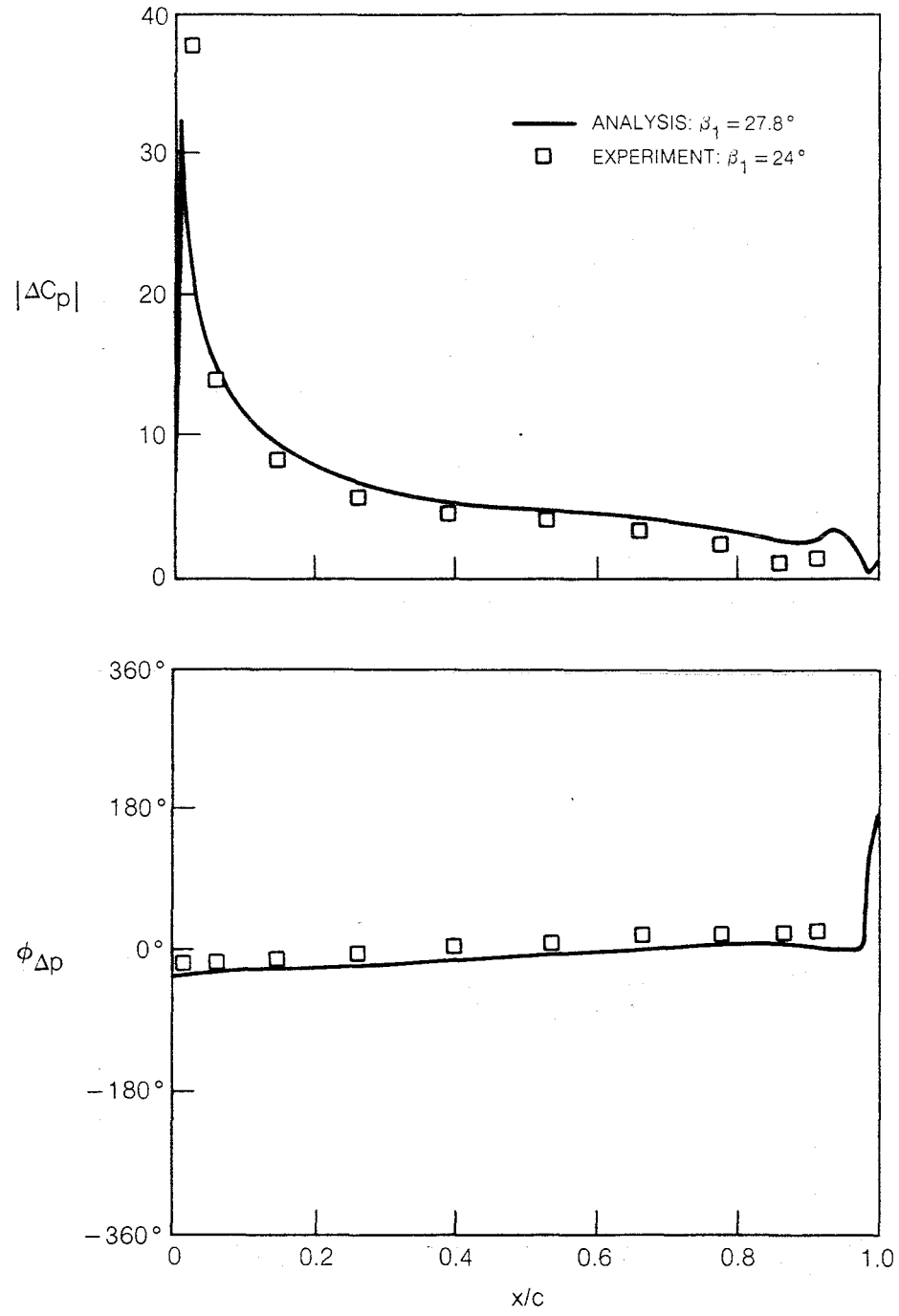

Fig. 4 Unsteady Pressure-Difference Coefficient for the First Standard Configuration; $M_1 = 0.17$, $\alpha = 2$, $k = 0.122$, $\sigma = -135°$.

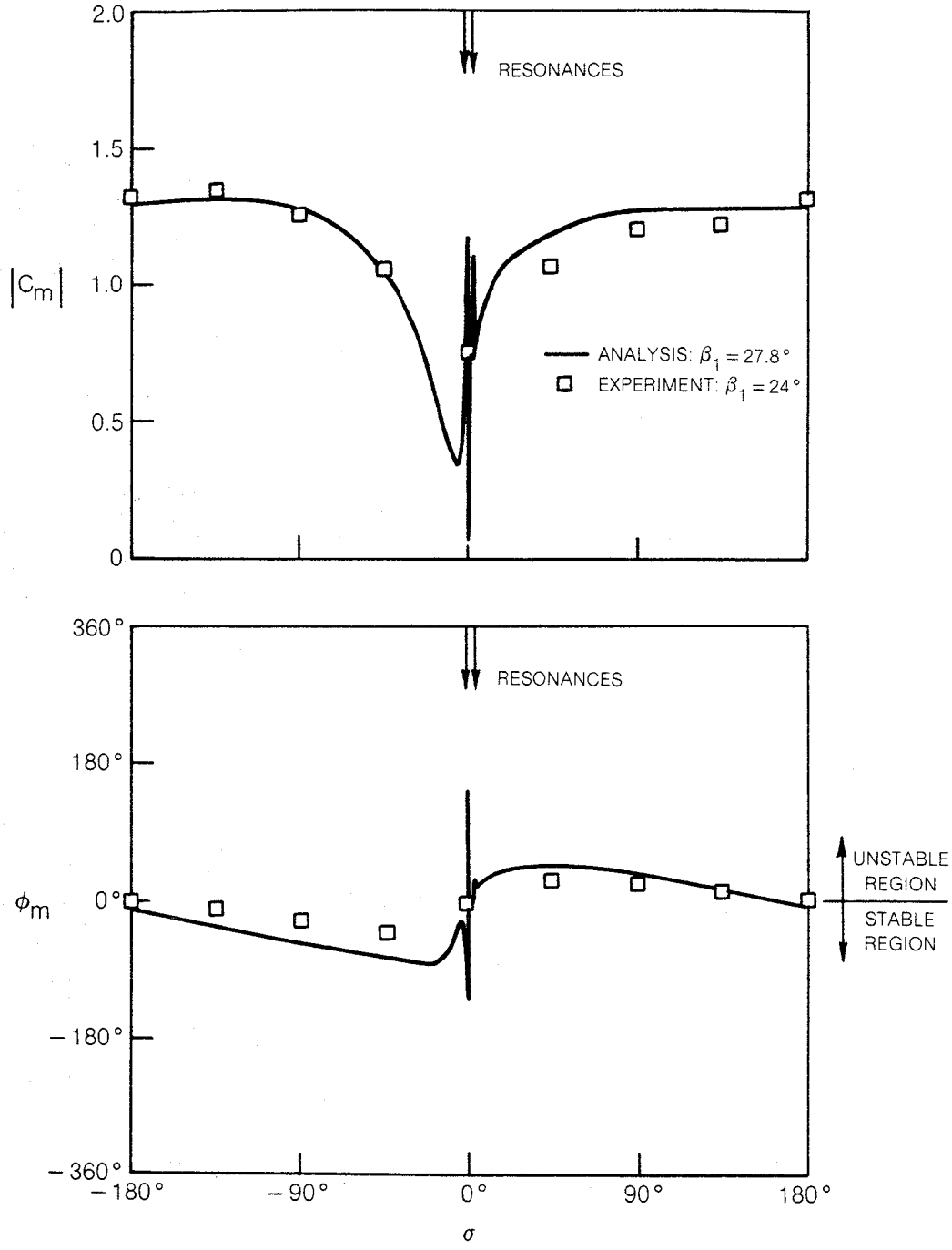

Fig. 5 Unsteady Moment Coefficient for the First Standard Configuration; $M_1 = 0.17$, $\alpha = 2°$, $k = 0.122$.

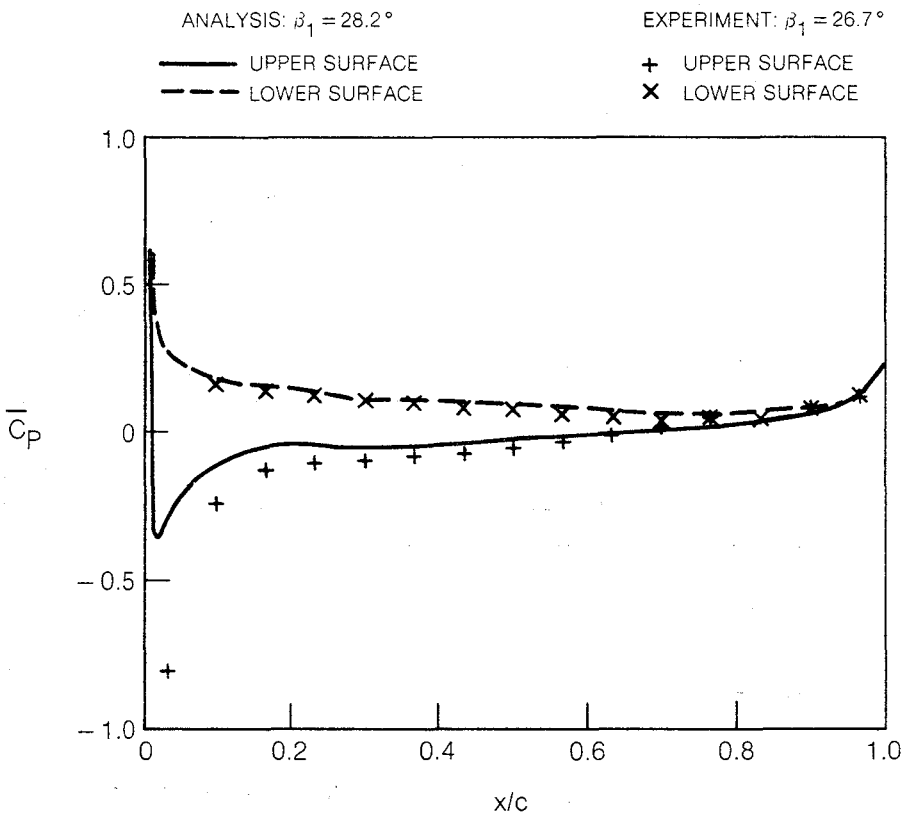

Fig. 6 Mean Surface-Pressure Coefficient for the Fifth Standard Configuration; $M_1 = 0.5$.

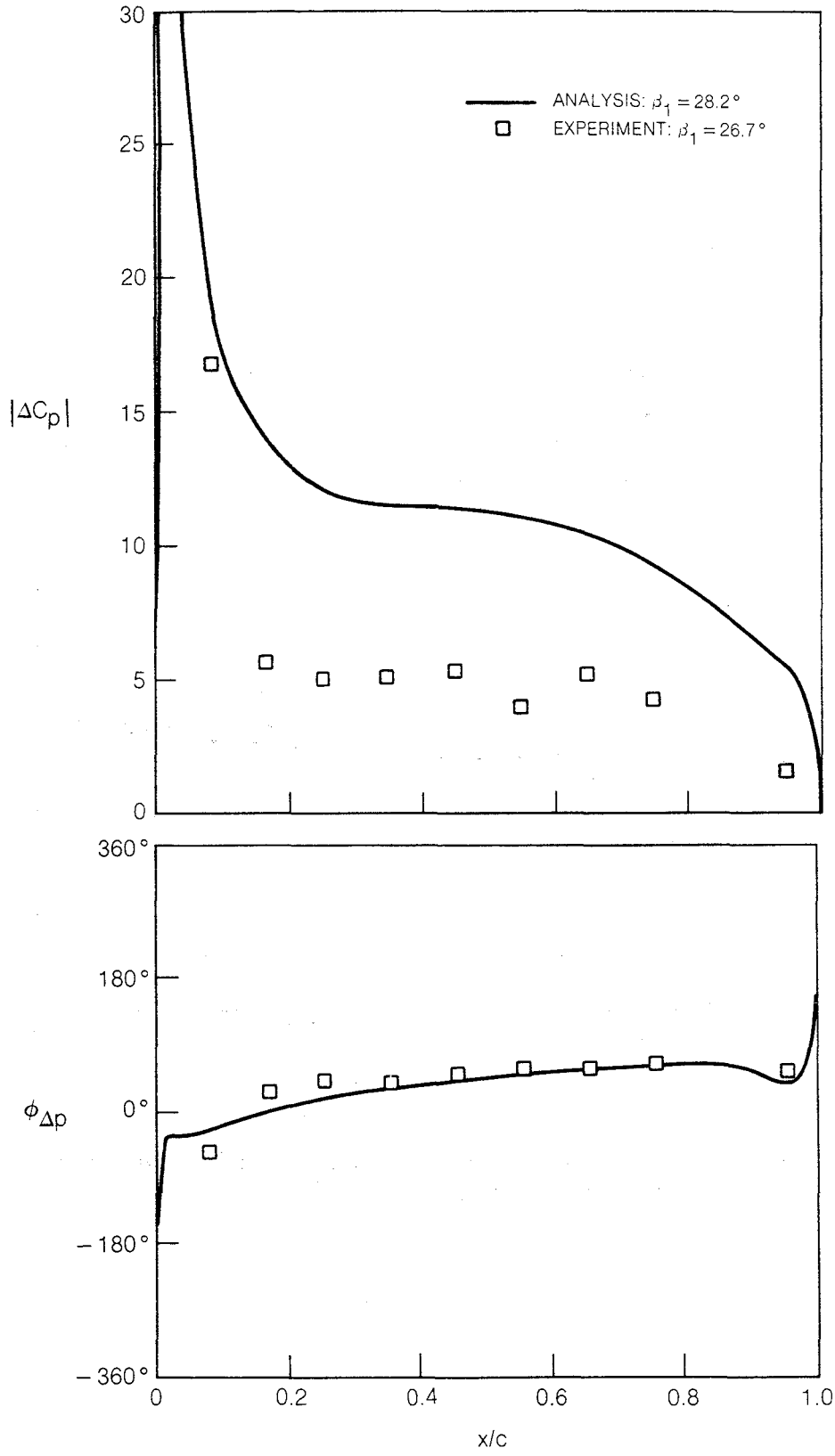

Fig. 7 Unsteady Pressure-Difference Coefficient for the Fifth Standard Configuration; $M_1 = 0.5$, $\alpha = 0.3°$, $k = 1.02°$, $\sigma = 180°$.

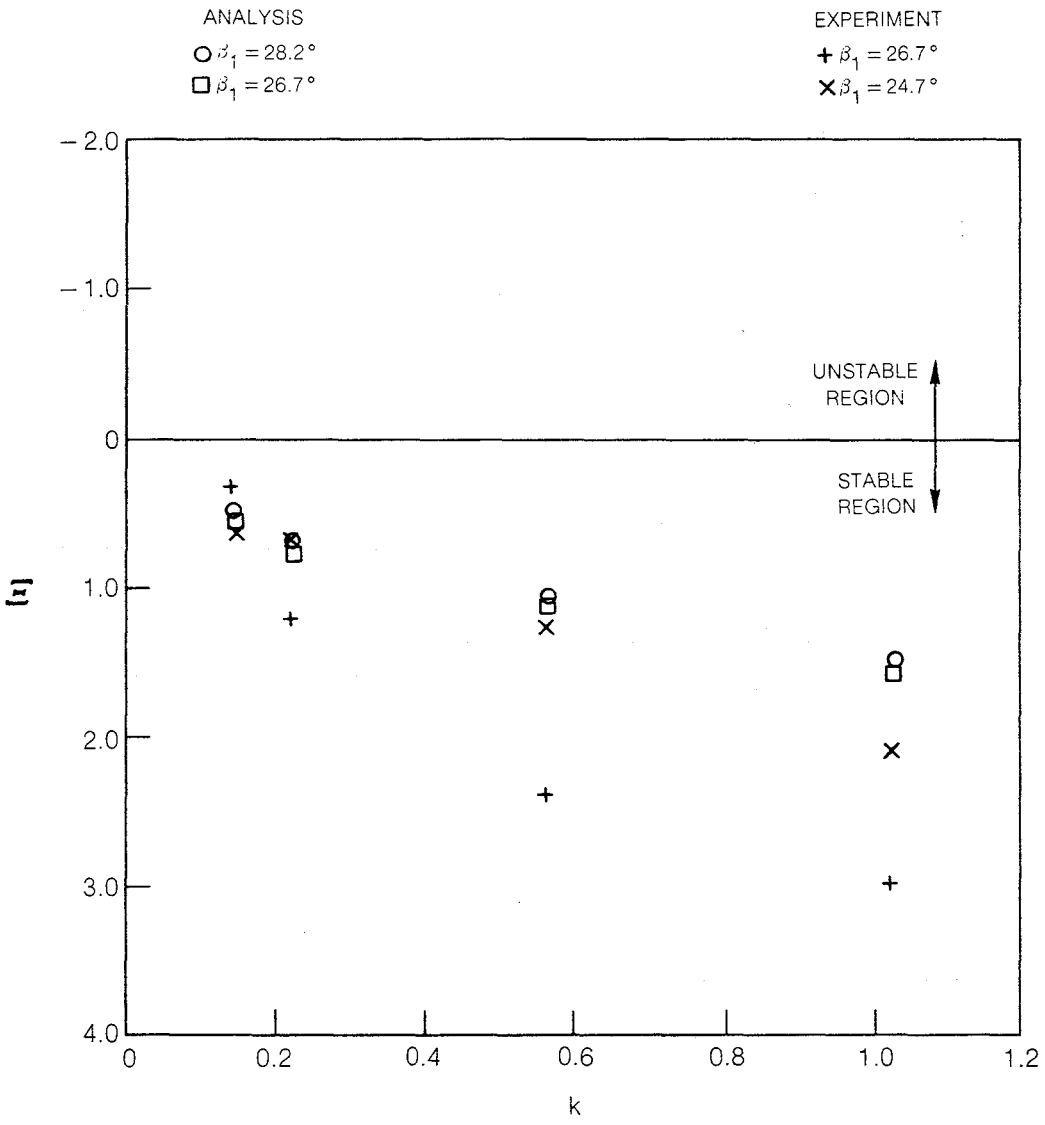

Fig. 8 Aerodynamic Damping Versus Reduced Frequency for the Fifth Standard Configuration; $M_1 = 0.5$, $\alpha = 0.3°$, $\sigma = 180°$.

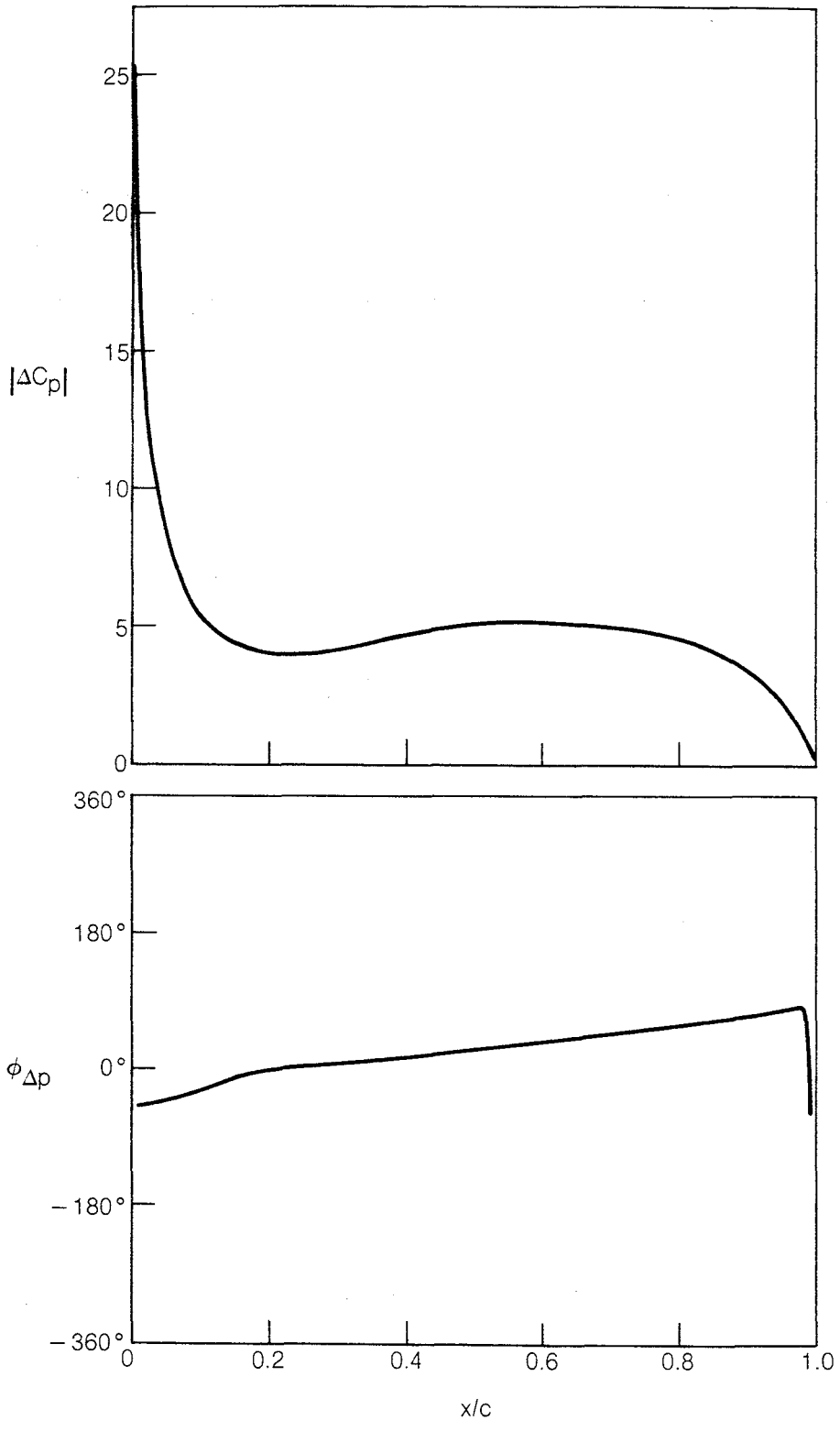

Fig. 9 Unsteady Pressure-Difference Coefficient for the Eight Standard Configuration; $M_1 = 0.8$, $\beta_1 = \theta = 30°$, $k = 1.0$, $\sigma = 90°$.

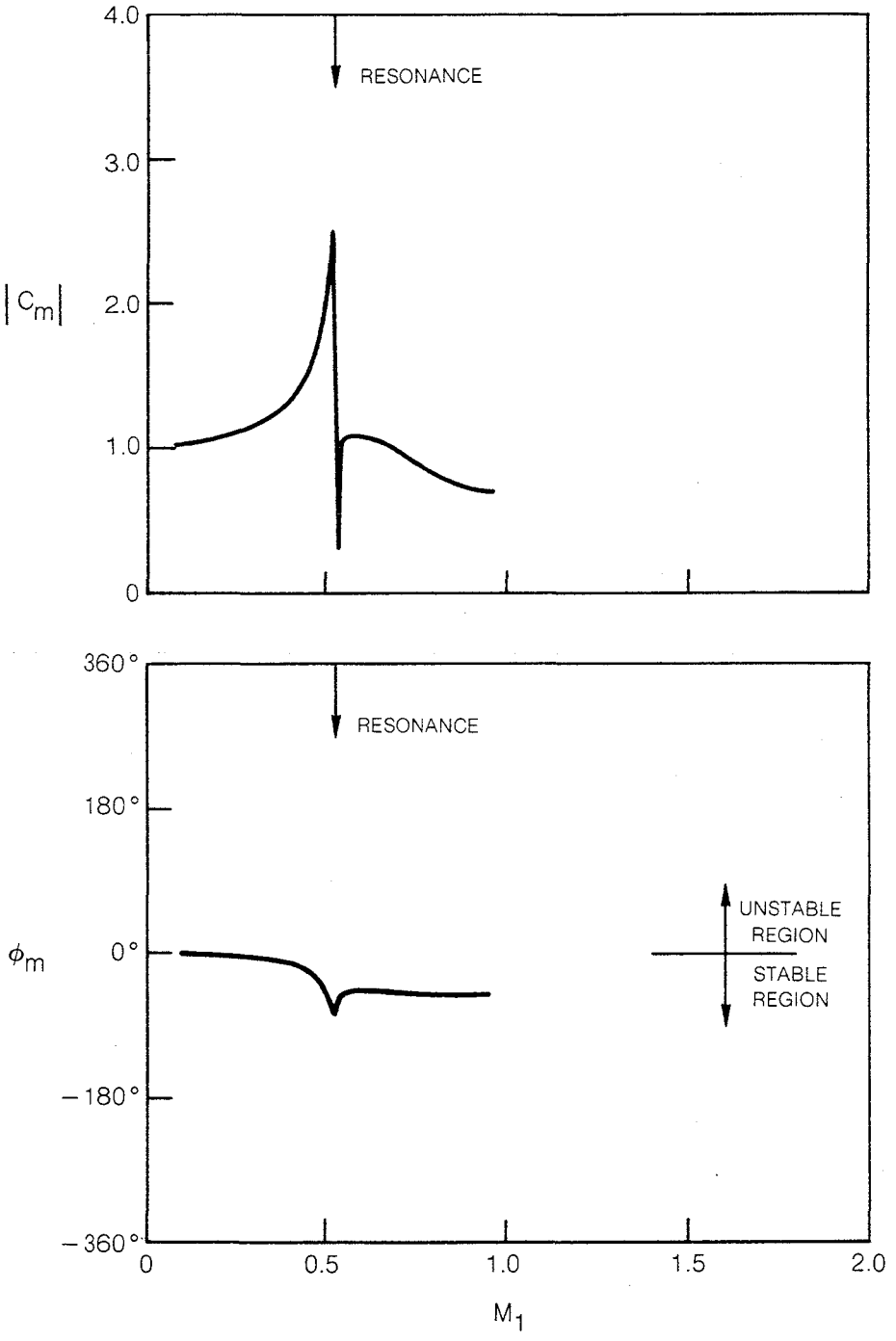

Fig. 10 Unsteady Moment Coefficient Versus Inlet Mach Number for the Eighth Standard Configuration; $\beta_1 = \theta = 30°$, k = 1.0, $\sigma = 90°$.

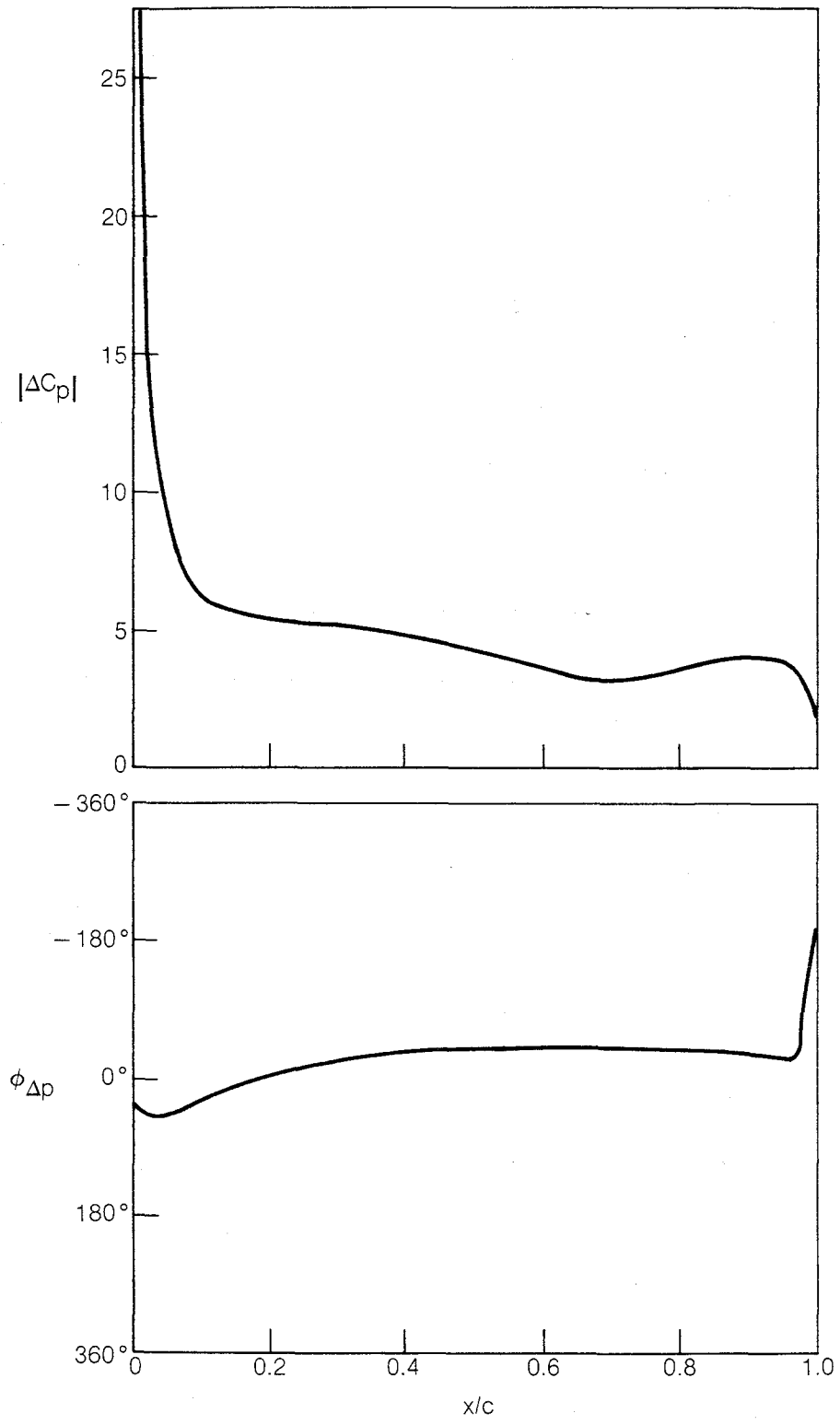

Fig. 11 Unsteady Pressure-Difference Coefficient for the Ninth Standard Configuration (2% Thick Symmetric Blades); $M_1 = 0.8$, $\theta = 30°$, $\beta_1 = 29.2°$, $k = 1.0$, $\sigma = 90°$.

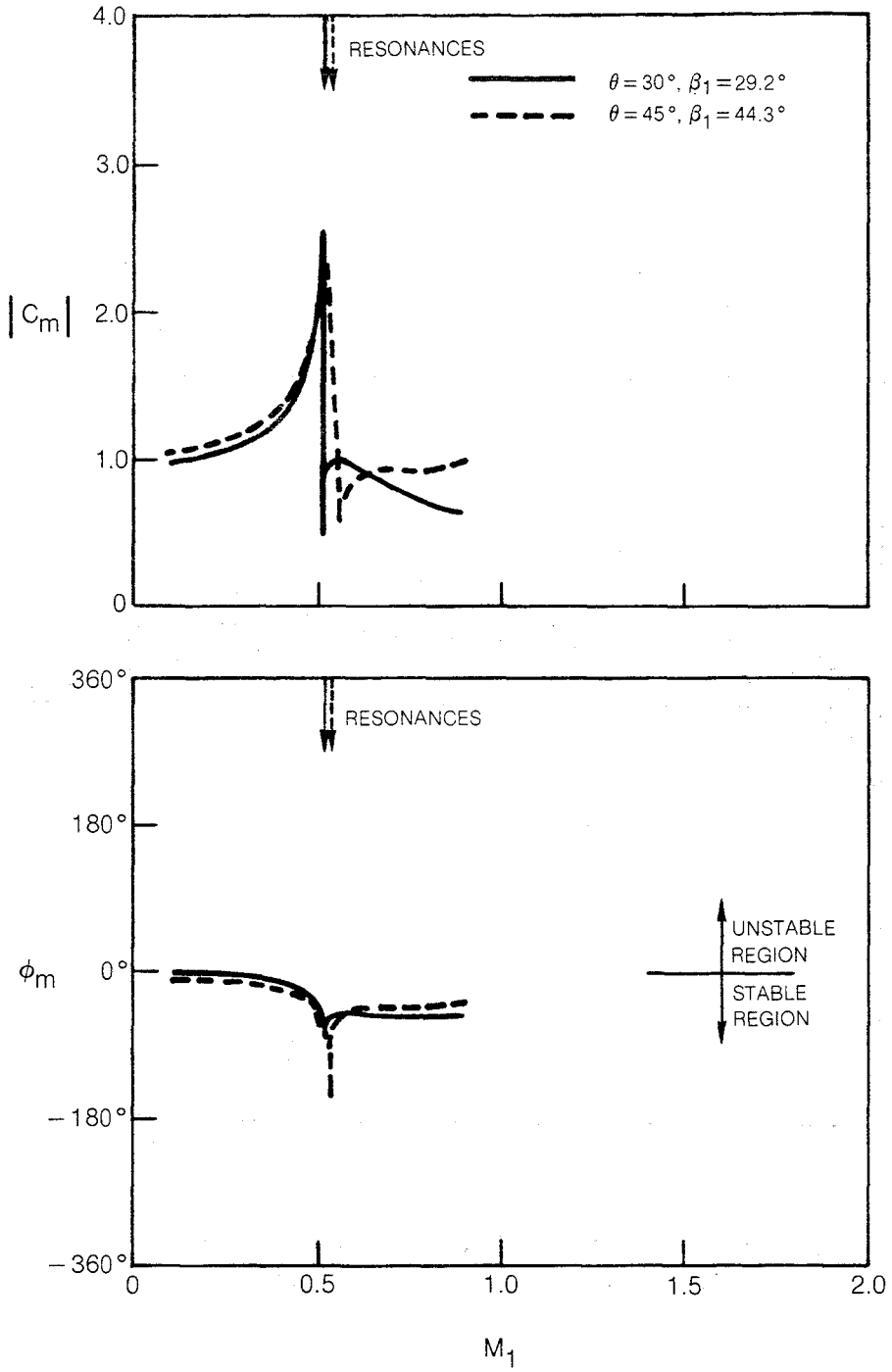

Fig. 12 Unsteady Moment Coefficient Versus Inlet Mach Number for the Ninth Standard Configuration (2% Thick Symmetric Blades); k = 1.0, $\sigma = 90°$.

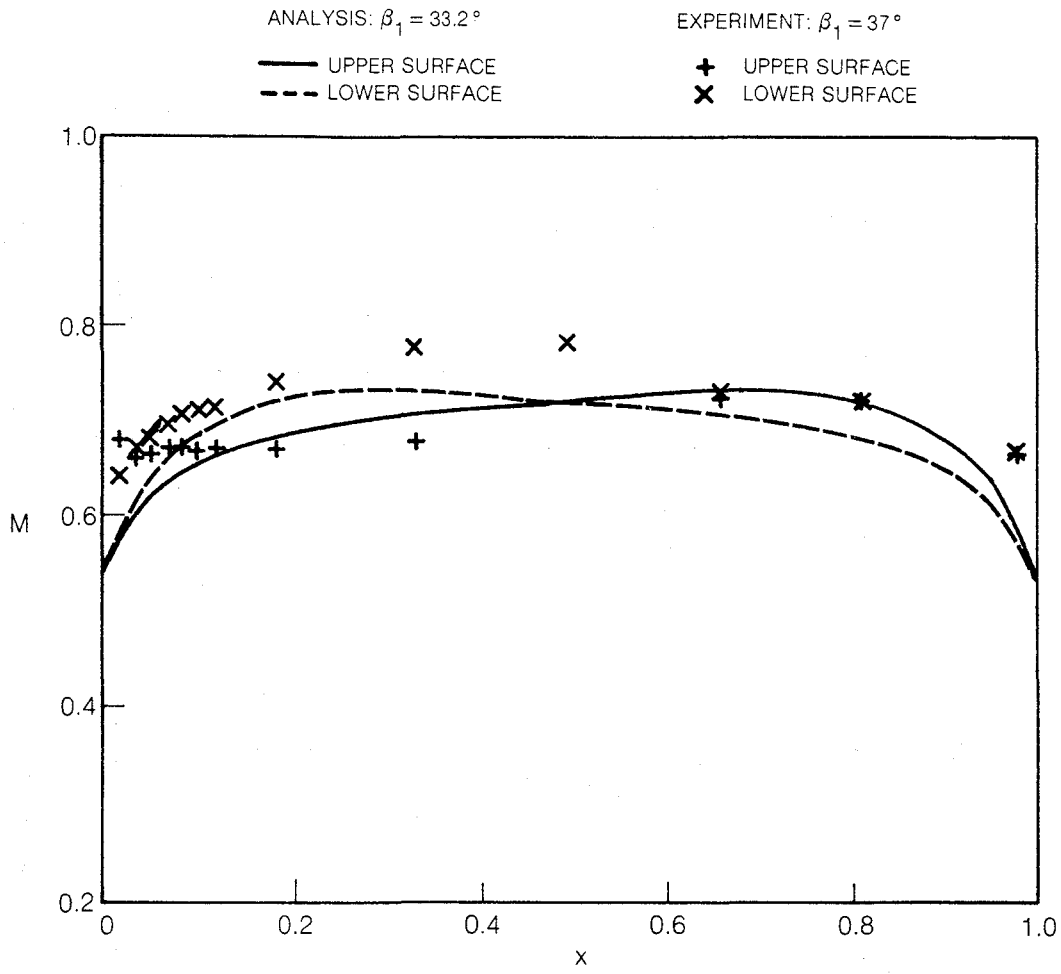

Fig.13 Steady Surface Mach Number Distributions for the NASA Lewis Cascade; $M_1 = 0.65$.

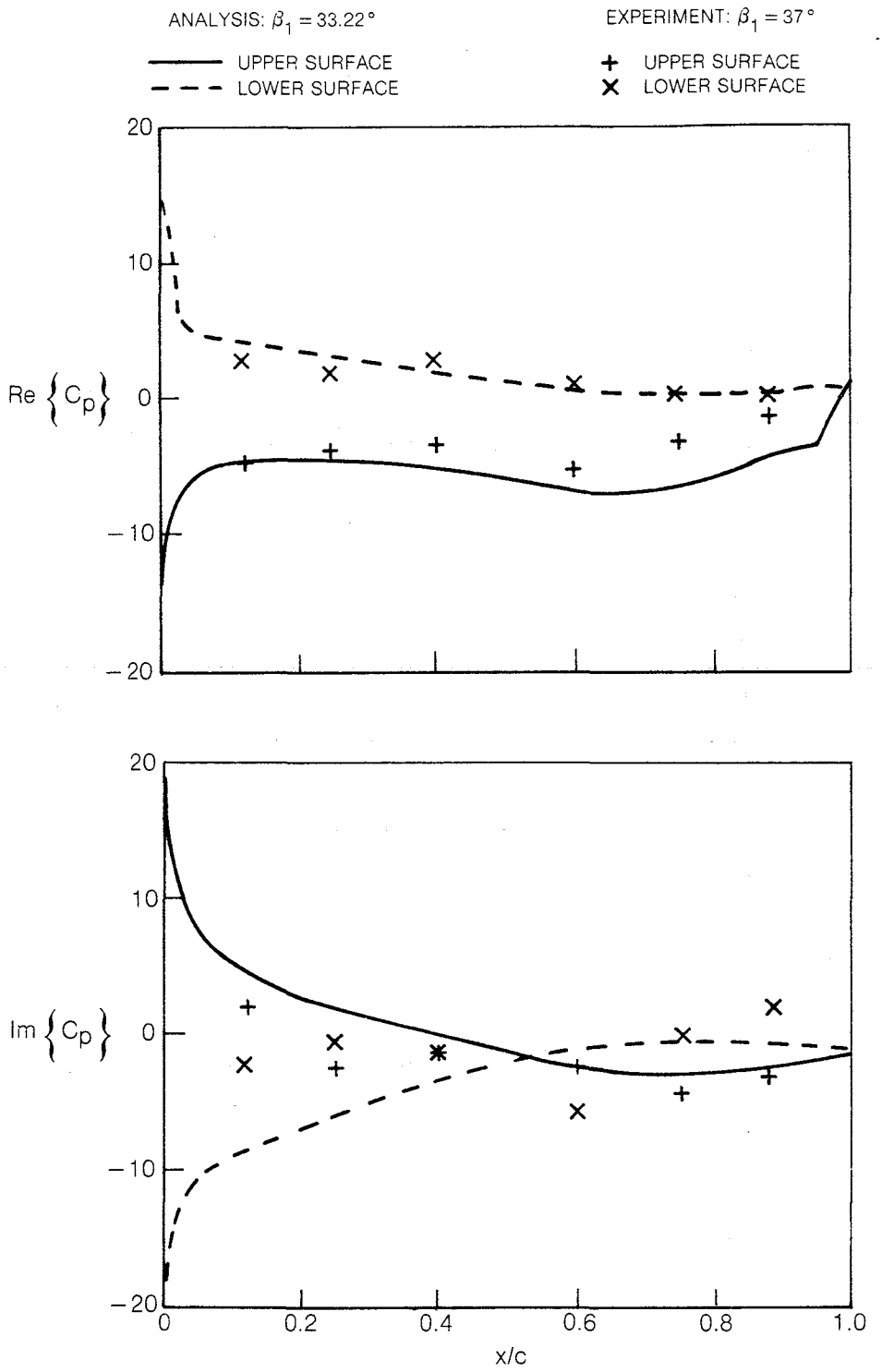

Fig. 14 Unsteady Surface-Pressure Coefficient for the NASA Lewis Cascade; $M_1 = 0.65$, $\omega = 200$ Hz, $\sigma = -90°$.

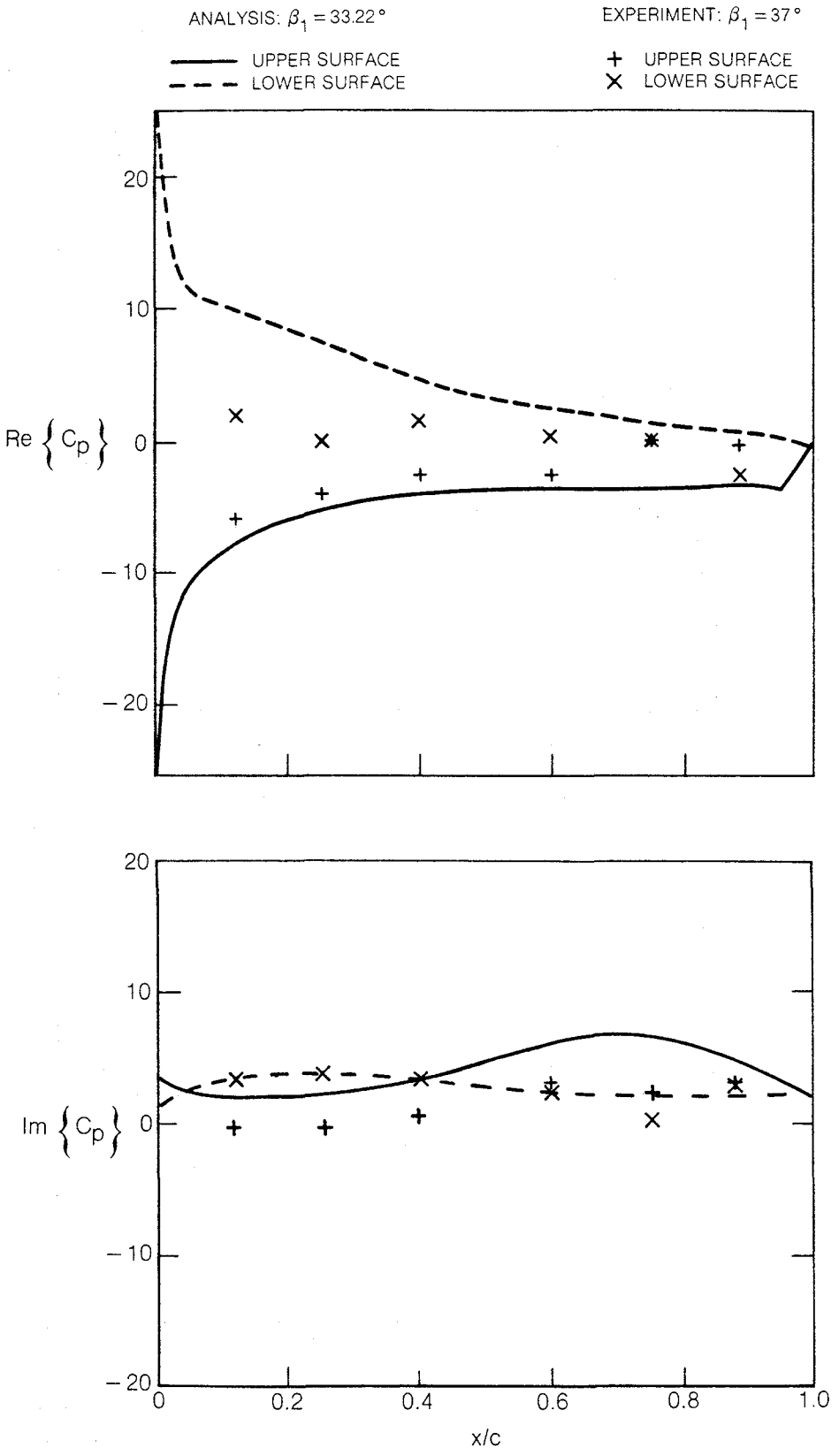

Fig. 15 Unsteady Surface-Pressure Coefficient for the NASA Lewis Cascade; $M_1 = 0.65$, $\omega = 200$ Hz, $\sigma = 90°$.

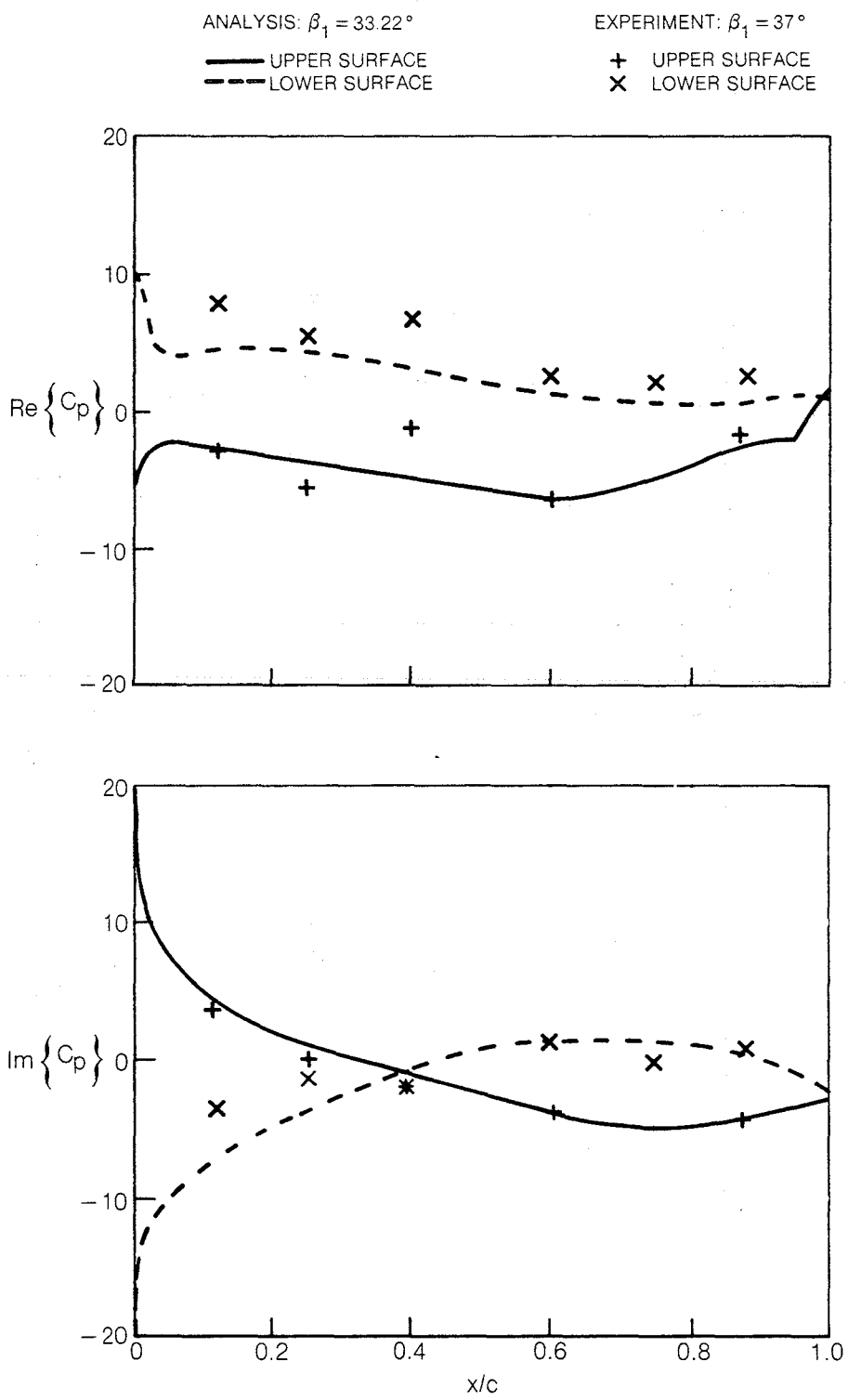

Fig. 16 Unsteady Surface-Pressure Coefficient for the NASA Lewis Cascade; $M_1 = 0.65$, $\omega = 500$ Hz, $\sigma = -90°$.

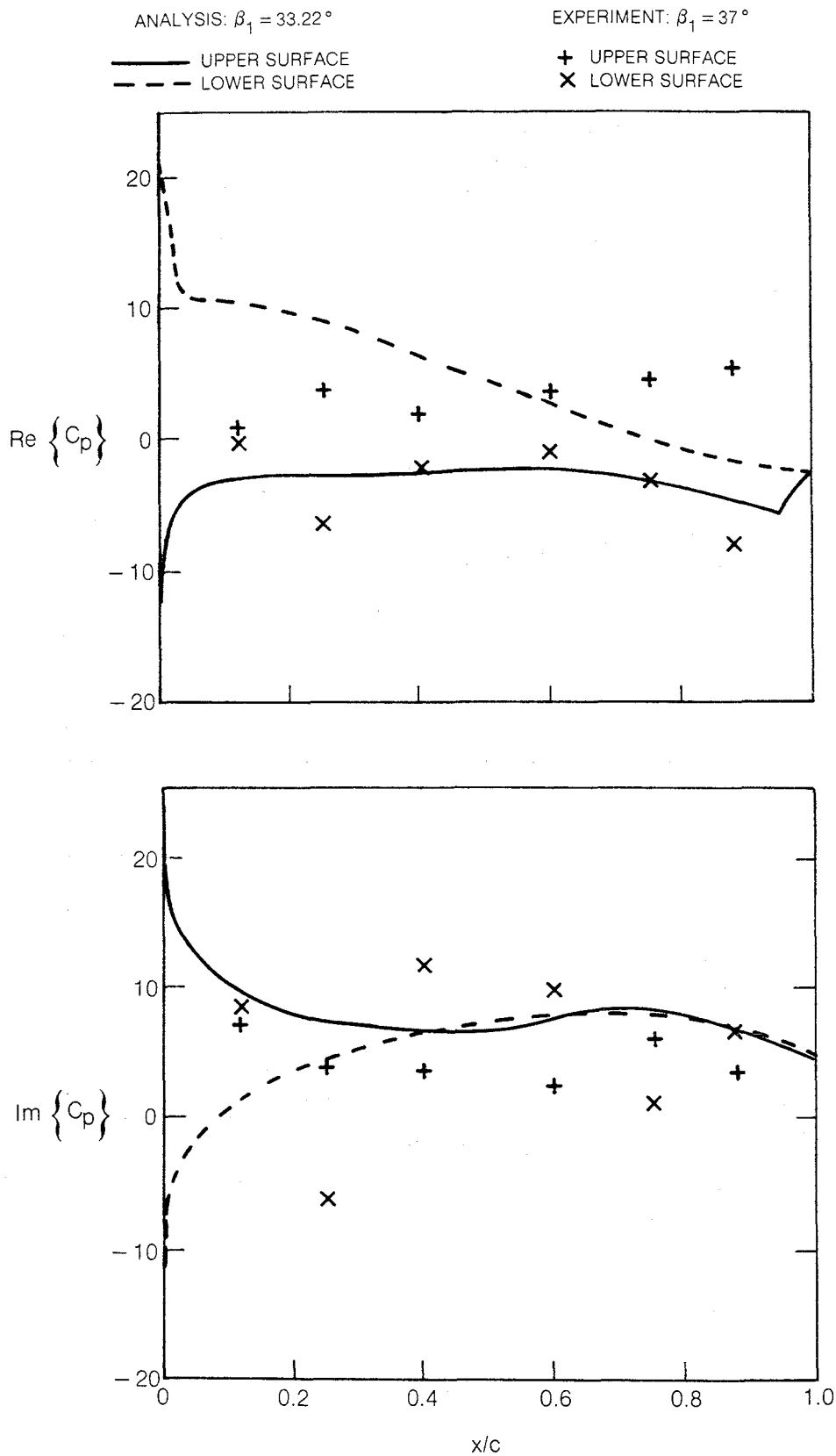

Fig. 17 Unsteady Surface-Pressure Coefficient for the NASA Lewis Cascade; $M_1 = 0.65$, $\omega = 500$ Hz, $\sigma = 90°$.

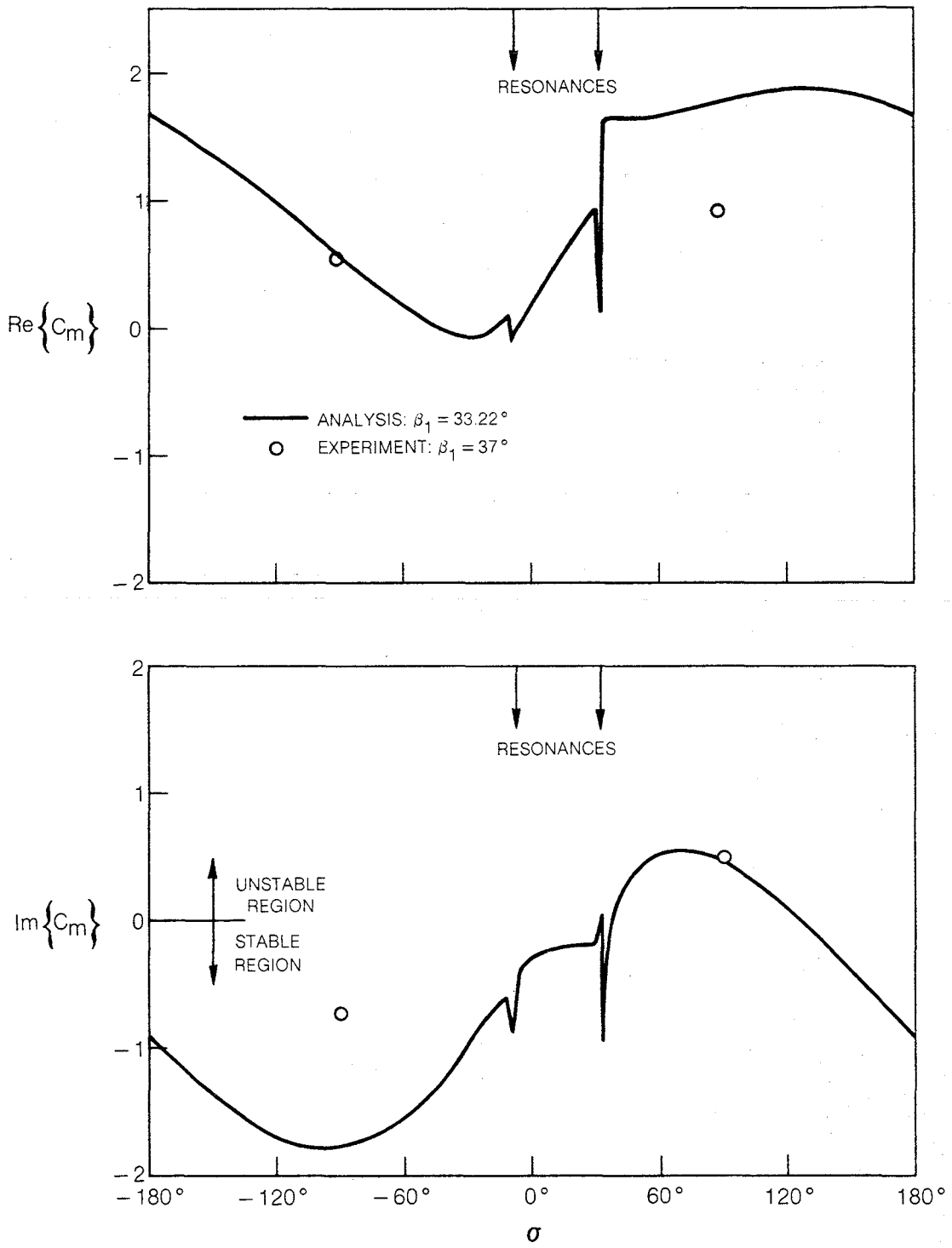

Fig. 18 Unsteady Moment Due to Torsion About Midchord for the NASA Lewis Cascade; $M_1 = 0.65$, $\omega = 200$ Hz.

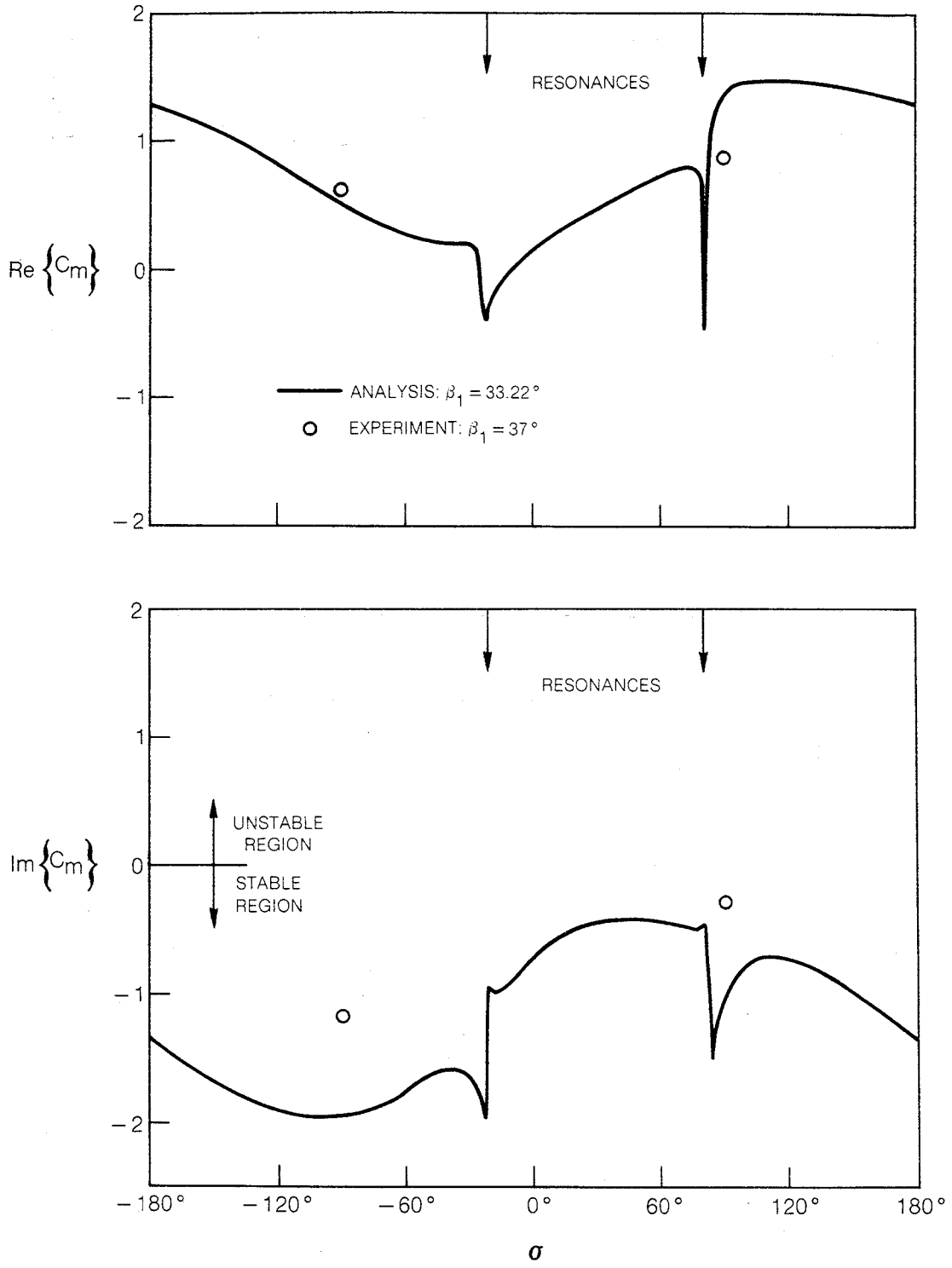

Fig. 19 Unsteady Moment Due to Torsion About Midchord for the NASA Lewis Cascade; $M_1 = 0.65$, $\omega = 500$ Hz.

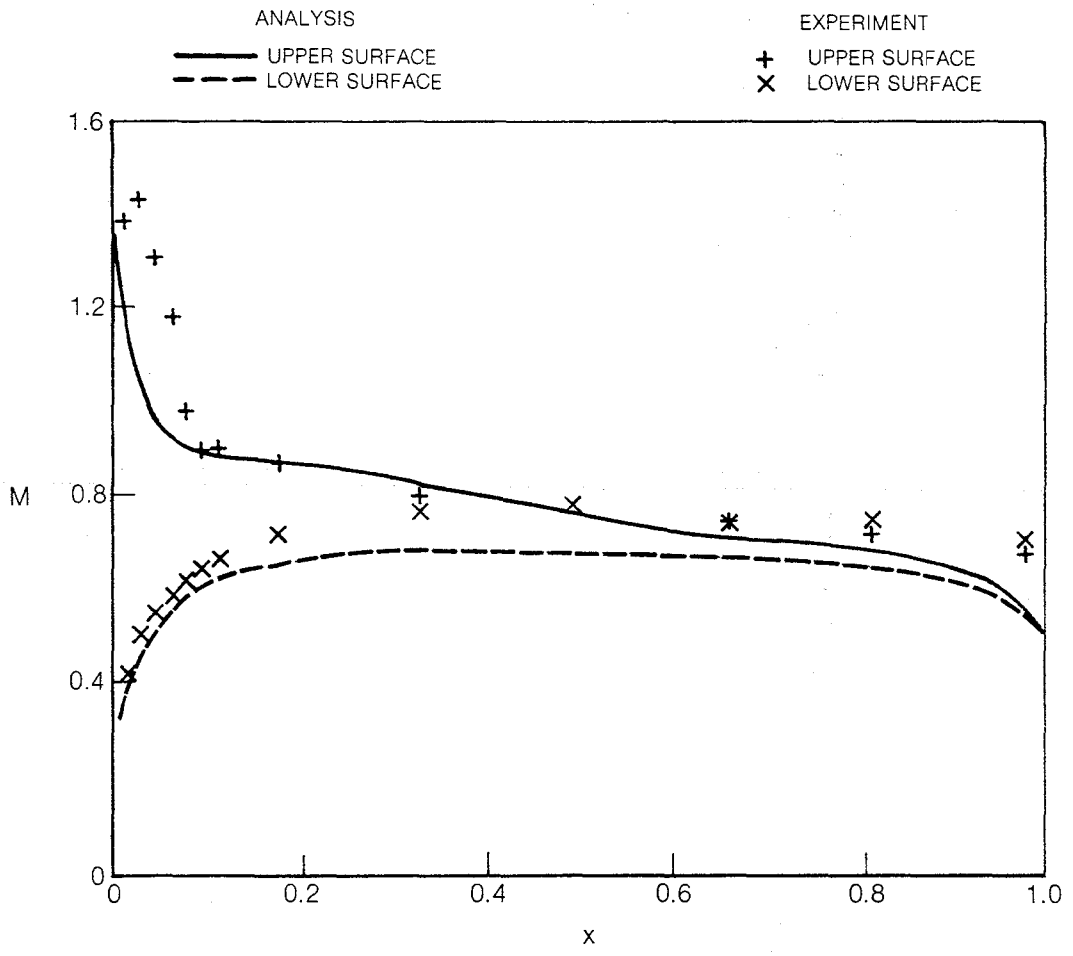

Fig. 20 Steady Surface Mach Number Distributions for the NASA Lewis Cascade; $M_1 = 0.8$, $\beta_1 = 30°$.

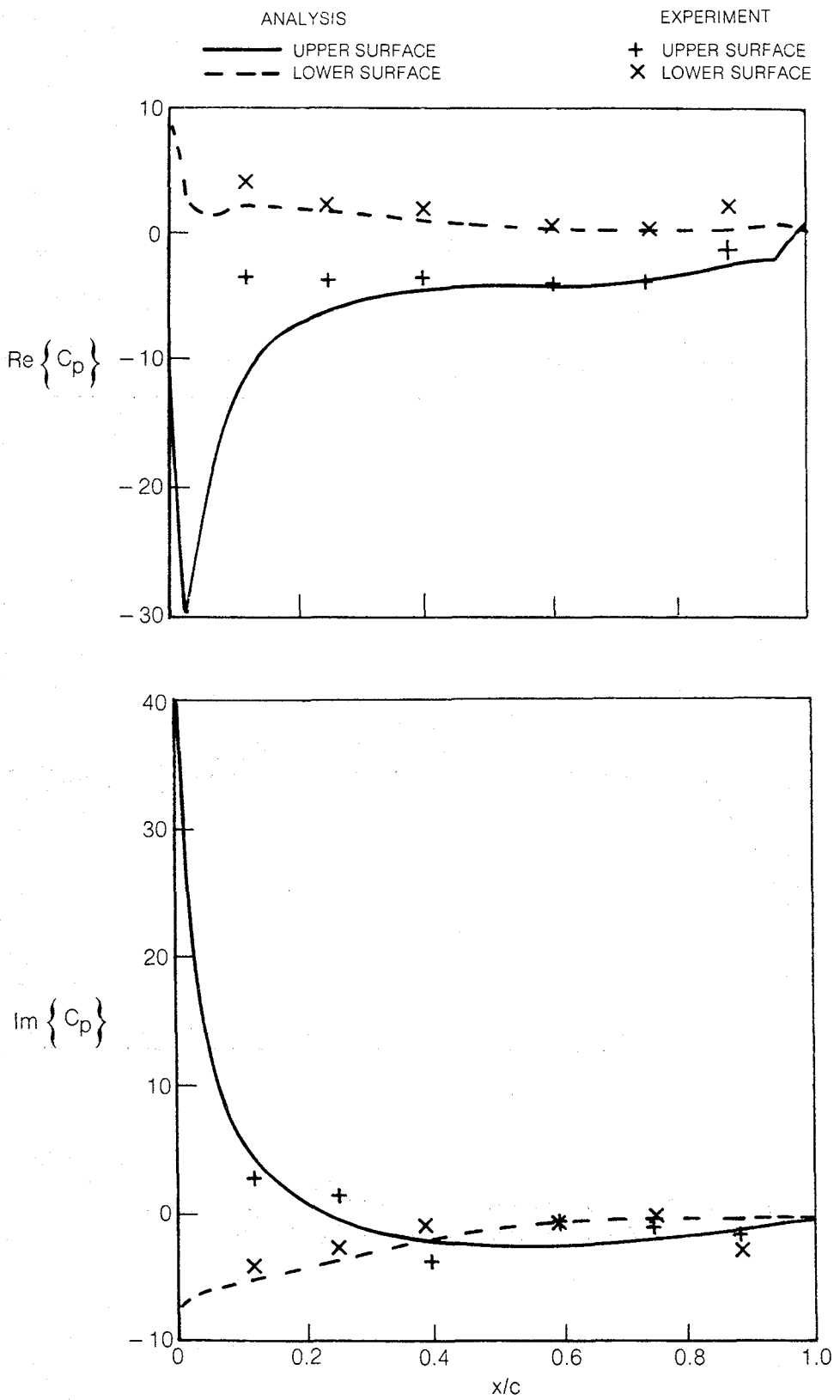

Fig. 21 Unsteady Surface-Pressure Coefficient for the NASA Lewis Cascade; $M_1 = 0.8$, $\beta_1 = 30°$, $\omega = 200$ Hz, $\sigma = -90°$.

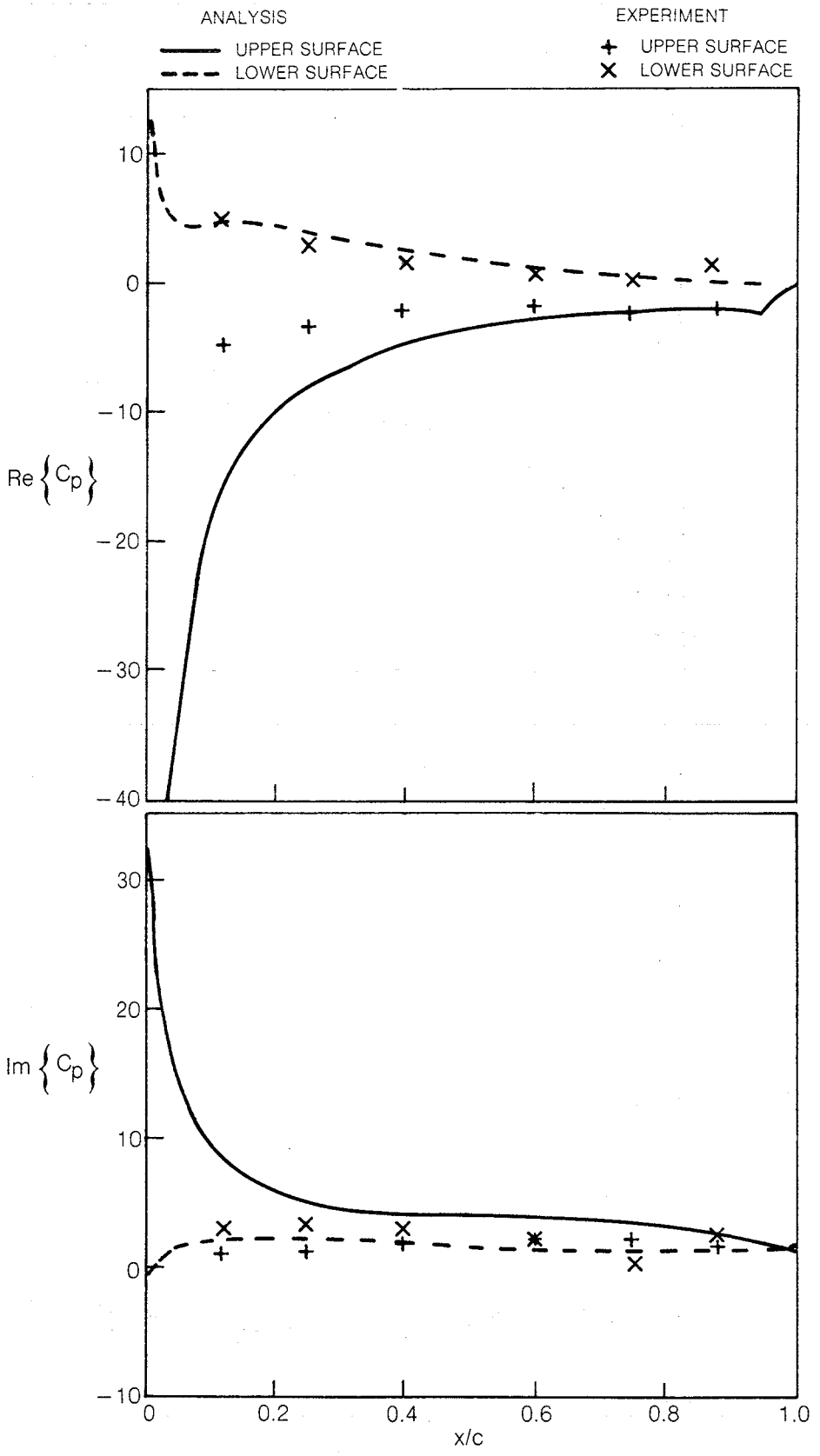

Fig. 22 Unsteady Surface-Pressure Coefficient for the NASA Lewis Cascade; $M_1 = 0.8$, $\beta_1 = 30°$, $\omega = 200$ Hz, $\sigma = 90°$.

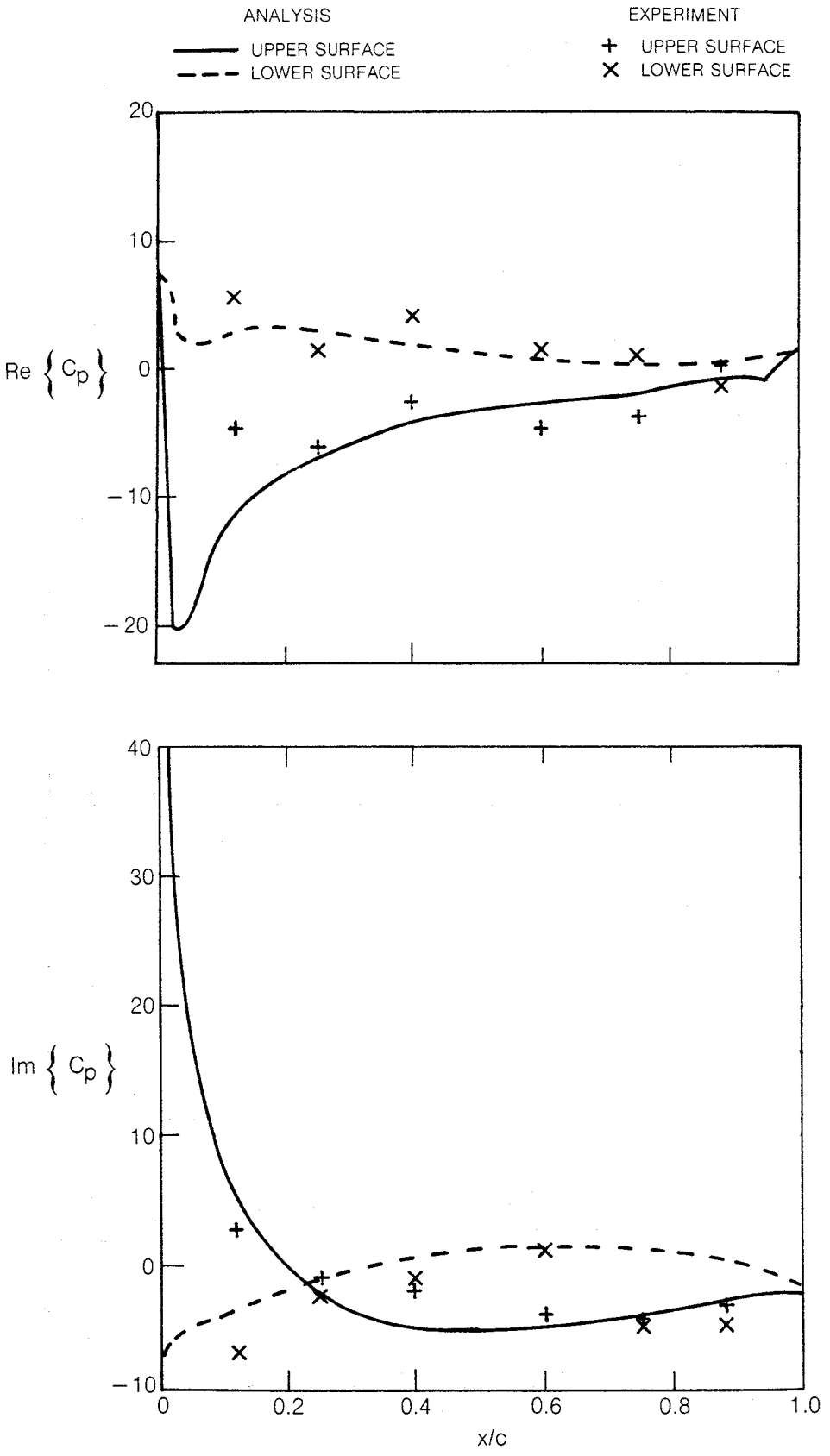

Fig. 23 Unsteady Surface-Pressure Coefficient for the NASA Lewis Cascade; $M_1 = 0.8$, $\beta_1 = 30°$, $\omega = 500$ Hz, $\sigma = -90°$.

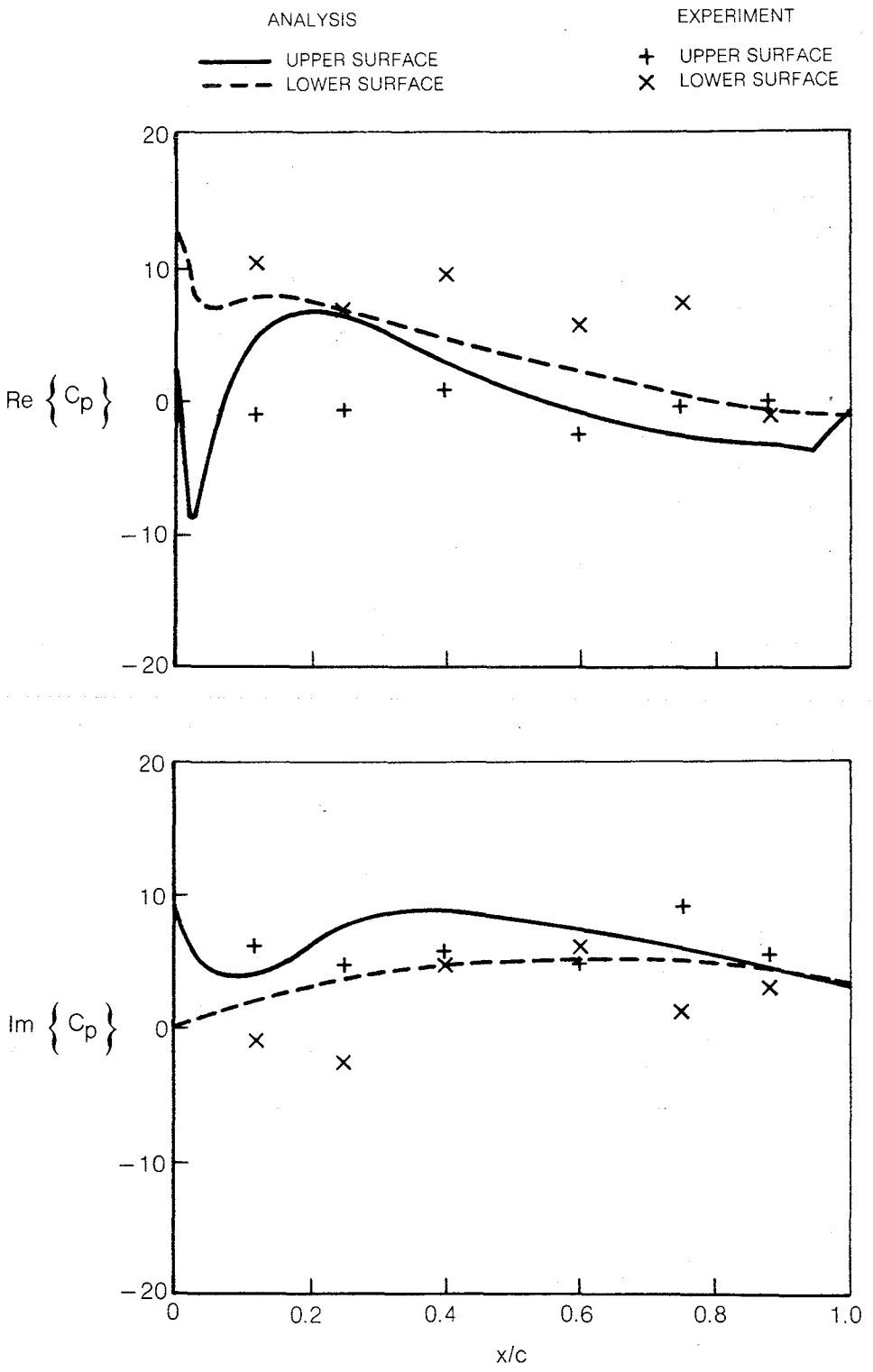

Fig. 24 Unsteady Surface-Pressure Coefficient for the NASA Lewis Cascade; $M_1 = 0.8$, $\beta_1 = 30°$, $\omega = 500$ Hz, $\sigma = 90°$.

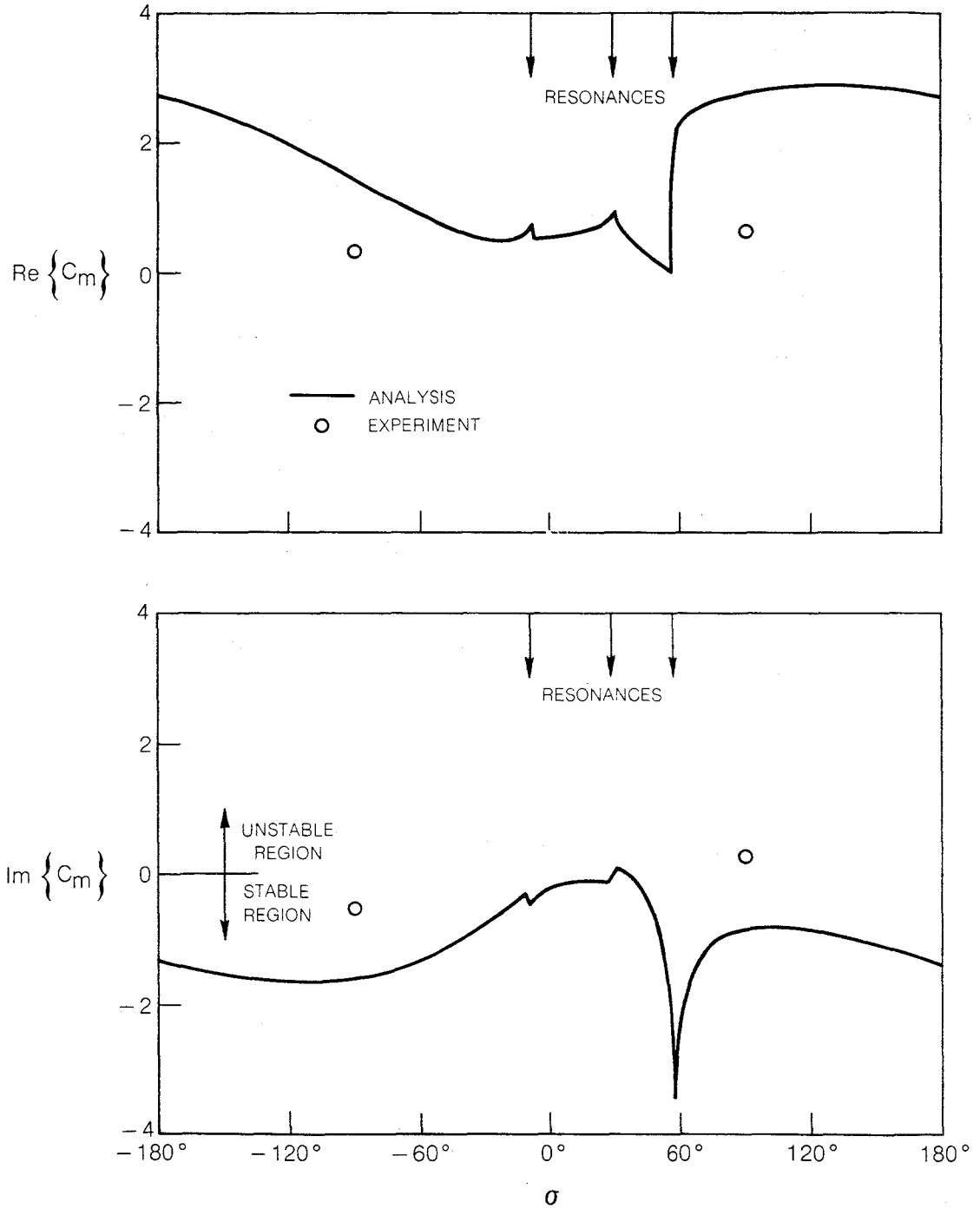

Fig. 25 Unsteady Moment Due to Torsion About Midchord for the NASA Lewis Cascade; $M_1 = 0.8$, $\beta_1 = 30°$, $\omega = 200$ Hz.

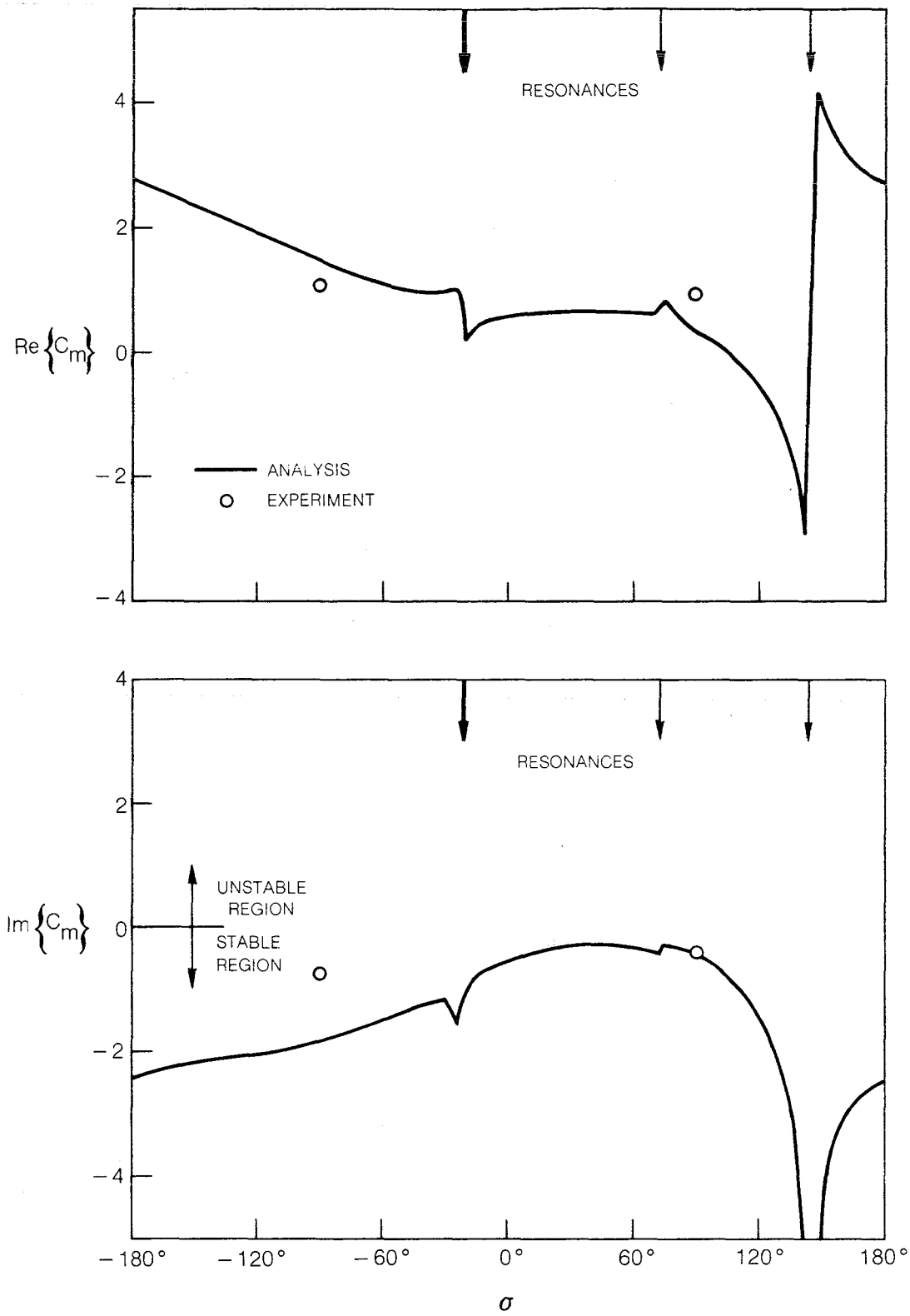

Fig. 26 Unsteady Moment Due to Torsion About Midchord for the NASA Lewis Cascade; $M_1 = 0.8$, $\beta_1 = 30°$, $\omega = 500$ Hz.

1. Report No.	2. Government Accession No.	3. Recipient's Catalog No.
NASA CR-3940		

4. Title and Subtitle	5. Report Date
Application of a Linearized Unsteady Aerodynamic Analysis to Standard Cascade Configurations	January 1986
	6. Performing Organization Code

7. Author(s)	8. Performing Organization Report No.
Joseph M. Verdon and William J. Usab, Jr.	R85-956896-4
	10. Work Unit No.

9. Performing Organization Name and Address	11. Contract or Grant No.
United Technologies Research Center Silver Lane East Hartford, Connecticut 06108	NAS3-22257
	13. Type of Report and Period Covered
12. Sponsoring Agency Name and Address	Contractor Report
National Aeronautics and Space Administration Washington, D.C. 20546	14. Sponsoring Agency Code
	505-45-58 (E-2686)

15. Supplementary Notes

Final report. Project Managers: Donald R. Boldman, Altitude Wind Tunnel Office, and Daniel Hoyniak, Advanced Turboprop Office, NASA Lewis Research Center, Cleveland, Ohio 44135.

16. Abstract

A linearized potential-flow analysis, which accounts for the effects of nonuniform steady flow phenomena on the linearized unsteady aerodynamic response to prescribed blade motions, has been applied to five cascade configurations. These include the first, fifth, eighth and ninth standard configurations proposed as a result of the Second International Symposium on Aeroelasticity in Turbomachines and a NASA Lewis flutter cascade. Selected results from this study, including comparisons between analytical predictions and the experimental measurements submitted for three of the foregoing configurations, are described in this report. The correlation between theory and experiment for the first standard configuration (a compressor cascade operating at low Mach number and frequency) is quite good. Moreover, the predictions and measurements for the NASA Lewis cascade of symmetric biconvex airfoils show good qualitative agreement. However, wide discrepancies exist between the theoretical predictions and the experimental measurements for the fifth standard configuration (a subsonic transonic fan-tip cascade). These can be partially attributed to conditions being imposed in the experiment which differ from those commonly used in unsteady aerodynamic analyses.

17. Key Words (Suggested by Author(s))	18. Distribution Statement
Linearized unsteady aerodynamics; Standard cascade configurations; NASA Lewis flutter cascade; Theoretical and experimental data base	Unclassified - unlimited STAR Category 02

19. Security Classif. (of this report)	20. Security Classif. (of this page)	21. No. of pages	22. Price
Unclassified	Unclassified	55	A04

For sale by the National Technical Information Service, Springfield, Virginia 22161

NASA-Langley, 1986

End of Document